AD-A128 282 TESTS OF SUBGRID-SCALE MODELS IN STRAINED TURBULENCE STUDIES OF THE STRUC..(U) NIELSEN ENGINEERING AND RESEARCH INC MOUNTAIN VIEW CA J H FERZIGER ET AL. 1/1

UNCLASSIFIED SEP 82 NEAR-TR-283 N00014-77-C-0008 F/G 12/1 NL

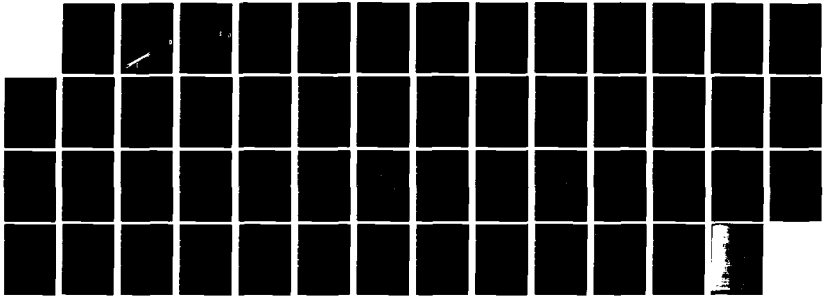

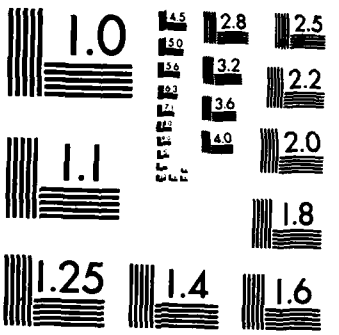

TESTS OF SUBGRID-SCALE MODELS IN STRAINED TURBULENCE and STUDIES OF THE STRUCTURE OF HOMOGENEOUS SHEAR FLOWS

by

J. H. Ferziger and O. J. McMillan

(12)

DEVELOPING A MODEL OF TURBULENCE NEAR A WALL FROM SOLUTIONS OF THE NAVIER-STOKES EQUATIONS.

by

D. R. Chapman and G. D. Kuhn

NIELSEN ENGINEERING AND RESEARCH, INC.

OFFICES: 510 CLYDE AVENUE / MOUNTAIN VIEW, CALIFORNIA 94043 / TELEPHONE (415) 968-9457

COPY NO. 92

TESTS OF SUBGRID-SCALE MODELS IN STRAINED TURBULENCE and STUDIES OF THE STRUCTURE OF HOMOGENEOUS SHEAR FLOWS

(12)

by

J. H. Ferziger and O. J. McMillan

DEVELOPING A MODEL OF TURBULENCE NEAR A WALL FROM SOLUTIONS OF THE NAVIER-STOKES EQUATIONS.

by

D. R. Chapman and G. D. Kuhn

NEAR TR 283

September 1982

Approved for public release; distribution unlimited

Prepared under Contract No. N00014-77-C-0008
ONR Task NR 061-244

for

OFFICE OF NAVAL RESEARCH
Washington, D.C.

by

NIELSEN ENGINEERING & RESEARCH, INC.
510 Clyde Avenue, Mountain View, CA 94043
Telephone (415) 968-9457

Unclassified

SECURITY CLASSIFICATION OF THIS PAGE (When Data Entered)

REPORT DOCUMENTATION PAGE		READ INSTRUCTIONS BEFORE COMPLETING FORM
1 REPORT NUMBER	2 GOVT ACCESSION NO. AD-A128282	3 RECIPIENT'S CATALOG NUMBER
4 TITLE (and Subtitle) (1) TESTS OF SUBGRID-SCALE MODELS IN STRAINED TURBULENCE (2) STUDIES OF THE STRUCTURE OF HOMOGENEOUS SHEAR FLOWS (3) DEVELOPING A MODEL OF TURBULENCE NEAR A WALL FROM SOLUTIONS OF THE NAVIER-STOKES EQUATIONS.		5 TYPE OF REPORT & PERIOD COVERED Final Report 11/1/76 - 7/31/82
		6 PERFORMING ORG. REPORT NUMBER NEAR TR 283
7 AUTHOR(s) (1)-(2) J. H. Ferziger and O. J. McMillan (3) D. R. Chapman and G. D. Kuhn		8 CONTRACT OR GRANT NUMBER(s) N00014-77-C-0008
9 PERFORMING ORGANIZATION NAME AND ADDRESS Nielsen Engineering & Research, Inc. 510 Clyde Avenue Mountain View, CA 94043		10 PROGRAM ELEMENT, PROJECT, TASK AREA & WORK UNIT NUMBERS NR 061 244
11 CONTROLLING OFFICE NAME AND ADDRESS Office of Naval Research Washington, D.C.		12 REPORT DATE September 1982
		13 NUMBER OF PAGES 47
14 MONITORING AGENCY NAME & ADDRESS(if different from Controlling Office)		15 SECURITY CLASS (of this report) Unclassified
		15a DECLASSIFICATION DOWNGRADING SCHEDULE N/A

16 DISTRIBUTION STATEMENT (of this Report)

Approved for public release; distribution unlimited.

17 DISTRIBUTION STATEMENT (of the abstract entered in Block 20, if different from Report)

18 SUPPLEMENTARY NOTES

19 KEY WORDS (Continue on reverse side if necessary and identify by block number)

Large-eddy simulation
Turbulence modeling

20 ABSTRACT (Continue on reverse side if necessary and identify by block number)

Three studies are described, each of which makes use of turbulent flow fields calculated using the Navier-Stokes equations. In the first study, exact numerical solutions of the full Navier-Stokes equations are used to evaluate subgrid-scale models used in large-eddy simulations. The flows investigated are homogeneous and incompressible with strong imposed mean strain or shear. Models evaluated include the conventional Smagorinsky

DD FORM 1 JAN 73 1473 EDITION OF 1 NOV 65 IS OBSOLETE

Unclassified

SECURITY CLASSIFICATION OF THIS PAGE (When Data Entered)

20. ABSTRACT (concluded)

model as well as a recently introduced formulation based on the notion of "scale similarity." In the second study, exact numerical simulations of homogeneous shear flows are examined using various computer-graphic tools, the aim being to attempt to understand the mechanisms underlying the production of turbulence energy and growth of length scales in such flows. The subject of the third study is the development of a computational model of the viscous sublayer of wall-bounded incompressible turbulent flow. In this work, the time-dependent Navier-Stokes equations, suitably simplified, are solved subject to boundary conditions imposed at the outer edge of the viscous sublayer. The formulation of these edge conditions so that computed average distributions of turbulence quantities agree with experimental data through the sublayer is the essence of this work.

PREFACE

This technical report covers the work performed under Contract N00014-77-C-0008 from 1 November 1976 to 31 July 1982 and is the fourth and summary technical report published under the program.

Dr. Robert Whitehead, Office of Naval Research, is the Navy Scientific Officer. Dr. Robert S. Rogallo of NASA/Ames Research Center has provided significant assistance, which is gratefully acknowledged as is the time provided to us on the Ames CDC 7600 computer.

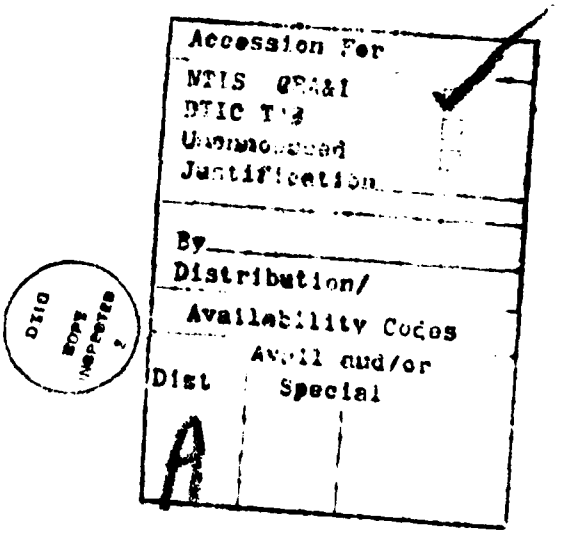

TABLE OF CONTENTS

1. INTRODUCTION

This is the Final Technical Report on a program conducted by Nielsen Engineering & Research, Inc. (NEAR) for the Office of Naval Research to investigate various aspects of the structure and computation of incompressible turbulence. Studies have been conducted over a five-year period in three main areas: (1) testing of subgrid-scale (SGS) models for use in large-eddy simulation (LES) of homogeneous turbulent flows; (2) investigations into the structure of homogeneous shear flow; and (3) developing a model of turbulence near a wall from solutions of the Navier-Stokes equations.

In the first two of these studies, we have been among the first investigators to use a technique which will assume increasing importance in the years to come: the use of full numerical solutions of the Navier-Stokes equations as "data" for model testing, determination of model parameters, and studies of the basic flow dynamical structure. For simple enough flows and if done with sufficient care, these full simulations (which use no models) can be considered exact representations. As such, they provide information on quantities of interest in unprecedented detail, and allow the study of quantities that currently cannot be measured experimentally. In our studies, we have used some of the full simulations of homogeneous flows done by Dr. Rogallo of the NASA/Ames Research Center (ref. 1).

The first study has involved the use of certain of these simulations as "data" to evaluate the models used in LES. In LES, the largest structures in the flow are computed directly using time-dependent three-dimensional equations derived from the Navier-Stokes equations by the application of a spatial filter. The filtering introduces terms involving the small-scale motions which must be modeled (the LES version of the turbulence closure problem). In our work, we have tested various SGS models by treating the results of Rogallo's full simulations as an experimentalist would treat measurements. The "data" from a

given time step in the full simulation are filtered to give the large-scale component of the flow field, and the small-scale field is obtained by subtraction. The terms which need to be modeled are then computed, as well as the model prediction of these terms using the large-scale field, and a direct comparison between the exact and modeled values is then made. The use of this approach to evaluate various forms of SGS models is isotropic turbulence and in turbulence interacting with mild strain was reported in references 2-4. The extension of this work to cases involving strong strain or shear is contained in reference 5 and in Section 2 of this report.

The second study undertaken under this research program also uses the full-simulation results of Rogallo as "data." In this investigation, attempts have been made to determine the mechanisms underlying the production of turbulence energy and growth of length scales in homogeneous shear flow using computer-generated displays of selected quantities as a form of "flow visualization." Progress achieved to date in this study is discussed in Section 3. Because most of the work to this point in this study has involved developing the computer-graphic tools required, only preliminary results are available at this time; this work is scheduled to be continued in another program under ONR sponsorship.

The aim of the third study is the development of a computational model of the viscous sublayer of wall-bounded incompressible turbulent flow. In this work, the time-dependent Navier-Stokes equations (simplified in accord with the experimental observations of the sublayer) are used to compute the characteristics in the sublayer subject to space- and time-dependent boundary conditions specified at the outer edge of the sublayer. The essence of this work is the formulation of these boundary conditions: experimental measurements have been used to guide their construction, and considerable success has been achieved with regard to the agreement with data of the resulting distributions throughout the sublayer of most of the important

turbulence quantities. This study is reported in reference 6 and Section 4 and will also be continued under ONR sponsorship.

2. TESTS OF SUBGRID-SCALE MODELS IN STRAINED TURBULENCE

In references 1 and 5, it is shown that Rogallo's full simulations of strained and sheared turbulence are representative of physical flows, as long as the simulations are not carried too far in time. The reasons for this are related to the fact that the computations are done using transformations of the independent and dependent variables, so that the physical coordinate system distorts as the computation proceeds. In Rogallo's simulation, the flow is divided into an imposed mean flow (U_i) and the turbulence (u_i). The mean flow is prescribed to be of the form:

$$U_i = \Gamma_{ik} x_k \tag{1}$$

and the solution of the equations for u_i (derived from the Navier-Stokes equations) is done after transformation of the independent and dependent variables:

$$\xi_i = B_{ik} x_k \quad \text{where} \quad \dot{B}_{ik} + B_{ij}\Gamma_{jk} = 0 \tag{2}$$

$$v_i = u_i / B_{ii} \quad \text{(no summation)} \tag{3}$$

Most of the solutions were done using 64 mesh points in each direction, although a few calculations (discussed later) were done using a 128^3 mesh; in either case, the calculations were done entirely in Fourier space.

For pure steady plane strain ($\Gamma_{11} = \Gamma$, $\Gamma_{22} = -\Gamma$, all other $\Gamma_{ij} = 0$) the result of the transformation (2) is that the computational region ultimately becomes very short in the 2-direction and the calculation must be stopped when the total strain ratio $e^{\Gamma t}$ reaches a value near 4. Continuing the calculations beyond this point results in the calculated flow becoming correlated in the compressed direction, which is of course unphysical.

Additionally, the distortion produces a grid for which all the wave numbers in the stretched direction represent relatively large scales, the dissipation range is not properly captured, and proper energy transfer is impeded. While strain ratios greater than four are often achieved experimentally (see, for example, ref. 7), a value of four is large enough to be useful. In the case of steady shear ($\Gamma_{12} = \Gamma$, all other $\Gamma_{ij} = 0$), the region shears and must periodically be readjusted. The readjustment causes some loss of information and requires that the results be treated carefully.

In most of the calculations used as a basis for model testing, plane strain was the force driving the turbulence away from isotropy. A number of shear cases were also run and no significant qualitative difference between shear and strain was found. Homogeneous shear of strength Γ can be regarded as a combination of plane strain of strength $\Gamma/2$ at 45° and rotation at angular velocity $\Gamma/2$. Since the effect of rotation is to reduce the production rate in the turbulence (cf. ref. 8), we expect the shear of strength Γ will produce effects similar to, but slightly weaker than strain of strength $\Gamma/2$; this is borne out by the calculations.

Since the earlier results of references 3 and 4 indicated that flows with low strain rates are not significantly different from isotropic turbulence and because most technological flows experience much higher strain rates, we decided to proceed by successively doubling the strain rate. In the end, the basic matrix contained four strain rates: 1.33, 2.65, 5.30, and 10.61 sec^{-1}. For each strain rate, the calculation was carried to total strain $e^{\Gamma t}$ of 1.3, 2, and 4. The initial Reynolds number R_λ was kept at 40 in all cases (the maximum available using Rogallo's simulation). Thus a total of twelve cases were available for analysis; of these, ten were actually analyzed. Several additional runs were made for special purposes. It is no surprise that the most interesting cases turned out to be the ones with the highest values of both strain rate and total strain.

To use the results of the full simulations in our studies of subgrid-scale modeling, the following definitions are required. The large-scale (filtered) velocity field is obtained from

$$\bar{u}_i = \int G(\underset{\sim}{r} - \underset{\sim}{r}')u_i(\underset{\sim}{r}')d\underset{\sim}{r}' \tag{4}$$

where G is a filter function which is usually chosen to be a Gaussian, $(\pi\Delta_a^2/6)^{-3/2}\exp(-6r^2/\Delta_a^2)$. In this work we use this filter with $\Delta_a/\Delta_c = 2$; Δ_c is the spacing of the grid on which the modeling is done. The subgrid-scale velocity field is then defined by $u_i' = u_i - \bar{u}_i$ and the subgrid Reynolds stress is defined by

$$\begin{aligned}\tau_{ij} &= \frac{1}{3}\delta_{ij}(2\overline{u_k'\bar{u}_k} + \overline{u_k'u_k'}) - \overline{u_i'\bar{u}_j} \\ &\quad - \overline{\bar{u}_i u_j'} - \overline{u_i'u_j'} = \frac{1}{3}\delta_{ij}R_{kk} - R_{ij}\end{aligned} \tag{5}$$

We will also look separately at the term

$$\tilde{\tau}_{ij} = \frac{1}{3}\delta_{ij}\overline{u_k'u_k'} - \overline{u_i'u_j'} = \frac{1}{3}\delta_{ij}\tilde{R}_{kk} - \tilde{R}_{ij} \tag{6}$$

which has been called the backscatter term (ref. 9).

One can derive equations for the subgrid-scale Reynolds stresses; these are similar to the equations for the usual time-averaged Reynolds stresses that are commonly used in turbulence modeling. From these equations one can derive an equation for the subgrid-scale kinetic energy $\langle\overline{\bar{u}_i u_i'} + \overline{u_i'u_i'}/2\rangle$. The production term in this equation is $\langle\overline{\tau_{ij}\partial\bar{u}_i/\partial x_j}\rangle$ and is the energy transfer from the large to small scales. We have computed this term and additionally have separated the contributions from τ_{ij} and $\tilde{\tau}_{ij}$. These results are shown in table 1 for two flow fields with a strain ratio of 4. Examination of $\langle\overline{\tau_{ij}\partial\bar{u}_i/\partial x_j}\rangle$ reveals that for the smaller of the two strain rates shown, the energy transfer is in the normal direction (to the small scales), but this reverses at the higher strain rate. Comparison with energy transfer via $\langle\overline{\tilde{\tau}_{ij}\partial\bar{u}_i/\partial x_j}\rangle$ shows that this reversal is due to the backscatter term, which for these two flows is transferring

energy from the small scales to the large ones. The energy transfer due to the "cross" or "outscatter" terms (the difference between $\langle \overline{\tau_{ij} \partial \bar{u}_i / \partial x_j} \rangle$ and $\langle \overline{\tilde{\tau}_{ij} \partial \bar{u}_i / \partial x_j} \rangle$) is seen to be in the normal direction for both flows of table 1 but is overwhelmed by the backscatter for $\Gamma = 10.61$ sec^{-1}, resulting in a net transfer of energy to the large scales. The behavior of the backscatter term is shown in figure 1 over the whole range of strain ratios covered for the two strain rates of table 1. Energy transfer from the small scales to the large scales seems to be associated with high strain rates which act on the flow for a long time.

The existence of energy transfers from the subgrid-scale to the large scales has a considerable effect on the validity of the subgrid-scale models as will be shown in the next section. Repeat calculations with different initial conditions (but the same initial spectrum) have shown that this effect is not the consequence of peculiar initial conditions. To eliminate the possibility that this phenomenon is a computational effect, the highest strain-rate case was recomputed more accurately by Rogallo using a 128^3 mesh. The results for this case are also shown in table 1: it is clear that the energy transfer to the large scales persists in this more accurate calculation, and is in fact more vigorous. Limited tests were also made with an alternate filter definition (a sharp cut-off filter in wave space). These suggest that although the amount of energy transfer between scales is obviously dependent on the definition of the filter used and on its width, the gross direction of the energy transfer is not. In pseudo-spectral calculations of homogeneous shear flows, Shirani, et al. (ref. 10) have observed a similar phenomenon; in their cases, there was energy transfer from both small and large scales to the medium-sized eddies. These results, which are not in accord with the usual concept of the energy "cascade" towards ever-smaller scales, may be of considerable importance in turbulence modeling.

The methodology used to test the models, which is an extension of that of reference 11, is now briefly described. From the

velocity fields described previously, which we accept as exact realizations of a turbulent flow field, we can compute τ_{ij} (or $\tilde{\tau}_{ij}$) on a coarse grid ($\Delta_c = 4\Delta$) overlaid on the computational grid. Furthermore, we can compute model versions of these quantities which are based on parameters of the large-scale field. A direct test of the model is made by computing the correlation coefficient η on the coarse grid between the exact subgrid-scale Reynolds stress and the model for the stress itself (the "tensor level"), its divergence (the "vector level"), and its associated energy transfer (the "scalar level"). For models which depend linearly on a single constant, the correlation coefficients are independent of the model constant and thus provide an unbiased test of the model. The constant can then be found by least-squares fitting but it was found that matching the mean-square values of the model and the exact result produces more satisfactory results in most cases.

2.1 Eddy Viscosity Models

Almost all large-eddy simulation work to date has used eddy viscosity models in which the effect of the subgrid-scale on the large-scale turbulence is represented as:

$$\tau_{ij} = 2\nu_T \bar{S}_{ij} \tag{7}$$

where ν_T is the eddy viscosity. A number of formulations of the eddy viscosity have been given by various authors but experience with them and the direct tests of references 4, 5, and 11 have shown that there is in fact little to choose among the various possibilities. Although eddy viscosity models are superior in some ways to other models that have been suggested, they are far from ideal. We will need to make do with them until more accurate models are proposed and tested. Thus the first task is to extend the method of references 4 and 5 to the strain and shear flows described above. Discussion of other kinds of models will follow.

We will focus on a particular formulation of the eddy viscosity, the Smagorinsky model:

$$\nu_T = (C_S \Delta_a)^2 |\bar{S}| \tag{8}$$

where $|\bar{S}|$ is the mean strain of the large-scale field and Δ_a is the filter width.

In our previous work, for isotropic decay the correlation coefficient and model parameters were found to be functions of a single nondimensional parameter – the subgrid-scale Reynolds number R_{sgs}; time was found not to be important in this flow. The model parameter, but not the correlation coefficient, was also found to depend somewhat on the numerical method used for differentiation in the model calculations but this is a computational effect rather than a physical one. The presence of strain means that the strain rate, Γ, is also an important independent parameter. Since it is dimensionally inverse time, it can be nondimensionalized using a time scale and there are two obvious choices. The first is the actual time and the nondimensional quantity formed using it is Γt; $e^{\Gamma t}$, the total strain, is a parameter of obvious importance in these flows. The second time scale is one characteristic of the flow itself. The best choice is t_d, the dissipation time scale, the ratio of the turbulence kinetic energy to the dissipation rate. Since the Reynolds number is fixed in this work, we have two parameters with which to correlate the results.

In the Smagorinsky model it is not clear whether the imposed mean strain rate should be included in the model (in ν_T and $\bar{S}_{ij}$) or not. On the one hand, one can argue that in a large-eddy simulation it is difficult to distinguish the mean strain from the turbulent component. On the other hand, if we consider the homogeneous strain flows with very large imposed strain, rapid distortion theory is approximately correct and the state of the turbulence will depend primarily on the total strain $e^{\Gamma t}$. The model parameter will then be inversely proportional to the

imposed strain at large strain rates. We have therefore decided to test the model both with and without the mean strain included.

The scalar level correlation coefficients* for the Smagorinsky model are plotted as functions of the total strain ratio in figure 2. The results with and without mean strain in the model are essentially identical so that there is nothing to choose between them on this basis. The value for isotropic decay is shown for comparison. We see that the validity of the model becomes dubious at large total strains. The negative value of the correlation coefficient at large strains reflects in part the reversed direction of energy transfer remarked on earlier. These results were obtained using $\tilde{\tau}_{ij}$ rather than τ_{ij} but calculations obtained using τ_{ij} show no substantial differences.

The model parameter for the Smagorinsky model with the mean strain included is shown in figure 3; figure 4 shows the same quantity without the mean strain. Again the parameter calculated for isotropic decay is shown for comparison. The reduction in the model parameter at large strain rates when the mean strain is included in the model is the effect anticipated above. When the mean strain is excluded the model parameter is very nearly independent of the imposed mean strain rate. We thus conclude that it is better not to include the mean strain in the model but, as remarked earlier, this may be very difficult to do in a large-eddy simulation of an inhomogeneous shear flow. Perhaps a model similar to the two-term model proposed in reference 12 would have the kind of properties that we desire.

The behavior of the correlation coefficients is extremely disappointing and means that eddy viscosity models cannot be

*These correlation coefficients were calculated without removing the mean of the exact or modeled scalar; it is better statistical practice to correlate the exact and modeled values of $\bar{u}_i \partial\tilde{\tau}_{ij}/\partial x_j - \langle \bar{u}_i \partial\tilde{\tau}_{ij}/\partial x_j \rangle$. Doing this results in correlation coefficients which are lower than those shown by as much as 0.16, but the conclusions demonstrated by figure 2 are unaltered.

trusted in flows with appreciable mean strain. (Although we have studied only the Smagorinsky model here, similar results have been obtained for the other eddy viscosity models.)

Another way to see the inability of the model to represent the subgrid-scale stresses is shown in figures 5 and 6. These "scatter plots" show the exact vs. the modeled values of $\bar{u}_i \partial \tilde{\tau}_{ij}/\partial x_j$ on the coarse grid and clearly indicate that the problem is truly the lack of correlation between the model and the exact result; no simple change in the model will help. On this type of plot, exact agreement between the modeled and exact quantities would be represented by the plotted symbols falling on a line bisecting the first and third quadrants. This is obviously far from the case here. (These plots were produced on microfiche by the computer. In the shaded area, the symbols fell so close together that resolution of individual points was lost.) The model obviously does not represent the subgrid-scale turbulence accurately even at low strain rates; the correlation coefficient of .45 is actually not very high. We also made plots showing the relative directions of the principal axes of the model and the exact stress and found, as anticipated, that the two sets of axes appear to be essentially random with respect to each other.

These results may explain why the Smagorinsky model has not been very effective in computing inhomogeneous shear flows, especially the channel flow which has been computed by a number of authors (refs. 12-15). There is clearly a need for improvement in the models used. Recently, a new concept in modeling was introduced (ref. 16), and we have performed some preliminary tests on this model. Some of these results are presented in the next section; more comprehensive evaluation is to be reported in reference 17.

2.2 New Models

In reference 16, the idea is advanced that the major interaction between the large- and small-scale components is between

the smallest scales of the large-scale field and the largest scales of the small-scale field ("scale similarity"). Since $\bar{u}_i$ represents the large-scale component of the field, applying the filter again produced a field ($\bar{\bar{u}}_i$) still richer in the largest scales, and

$$\tilde{u}_i = \bar{u}_i - \bar{\bar{u}}_i \tag{9}$$

is a field which contains the smallest scales of the large-scale component. A simple version of a model which incorporates the notion of scale similarity is then

$$\tilde{\tau}_{ij} = C(\tfrac{1}{3}\delta_{ij}\tilde{u}_k\tilde{u}_k - \tilde{u}_i\tilde{u}_j) \tag{10}$$

Some exploratory results using equation (10) are shown in tables 2 and 3. In table 2, the correlation coefficients for this model in homogeneous isotropic turbulence at the tensor (comparison with $\tilde{\tau}_{ij}$), vector (comparison with $\frac{\partial\tilde{\tau}_{ij}}{\partial x_j}$), and scalar (comparison with $\bar{u}_i\frac{\partial\tilde{\tau}_{ij}}{\partial x_j}$) levels are given. Values for the Smagorinsky model are given for comparison and it is clear that the model of equation (10) has considerable promise. An even more impressive comparison is given in table 3 which presents the analogous quantities for strained turbulence. In these tables the correlation coefficients were calculated after removing the means (in contrast to those of fig. 2). A typical scatter plot is given in figure 7; the improvement over the previous results is obvious.

A version of the scale-similarity model which is seemingly even more accurate is described in reference 16:

$$\tau_{ij} = C\left[\tfrac{1}{3}(\bar{u}_k\bar{u}_k - \bar{\bar{u}}_k\bar{\bar{u}}_k)\delta_{ij} - (\bar{u}_i\bar{u}_j - \bar{\bar{u}}_i\bar{\bar{u}}_j)\right] \tag{11}$$

In that reference, correlation coefficients for isotropic and sheared turbulence are shown which are even higher than those for the model of equation (10) in tables 2 and 3.

The apparent success of these models led to a test in a large-eddy simulation by Bardina, et al. and they found that

these models are not dissipative. As a result, a search was made for models which contained the best features of the new models and the Smagorinsky model. Among the ideas that we tried was a Smagorinsky model with the large-scale velocity $\bar{u}_i$ replaced by $\tilde{u}_i$; the results were found to be very similar to those for the Smagorinsky model. Another idea was to model $\partial\tilde{\tau}_{ij}/\partial x_j$ directly in terms of $\tilde{u}_i$; this model was found to have almost no validity at all.

The suggestion was then made that a model which is a linear combination of the Smagorinsky model and equation (11) should have the best features of both models. Some promising preliminary tests of this concept have been made and investigation of combined models of this type has been continued (ref. 17).

3. STUDIES OF STRUCTURE OF HOMOGENEOUS SHEAR FLOWS

In the past decade, vortex pairing has been put forward as a primary mechanism for the growth of free-shear flows (particularly in the mixing layer) and other mechanisms of importance in other turbulent flows have begun to be recognized. Although it has not happened yet, these insights into the physics of turbulent flow are expected to have important influences on turbulence modeling. It is our intent to contribute to the understanding of the basic mechanisms underlying turbulent flows by making use of the wealth of information implicit in the flow fields calculated by full numerical simulation of the Navier-Stokes equations.

Our tools in this study are primarily visual: by making contour plots of various quantities of importance in these flows (e.g., turbulent stress or vorticity), we are attempting to find evidence of a mechanism akin to pairing to explain the length-scale growth which occurs when turbulence is strained or sheared. Specifically, we are focusing on the homogeneous shear flows calculated by Rogallo (ref. 1), treating them as "experimental data" measured in complete detail at a series of discrete time steps.

In the past year, we have developed the data-handling procedures and computer-graphics routines necessary to investigate the structure of homogeneous shear flows, and we have begun this study using one of Rogallo's calculated cases (ref. 1, case BSH9, shear rate $S = \partial\bar{u}/\partial y = 28$). These cases were computed in a coordinate system which shears with the mean motion, and which is remeshed periodically to avoid having the computational volume become too small in any direction to resolve the pertinent turbulent scales. Velocity fields are available for analysis at the instants of time at which the coordinate system is orthogonal ($St = 0,1,2,\cdots$). Rogallo's calculations were done on the ILLIAC computer at NASA/ARC using 128^3 grid points. Our data reduction and post-processing is done on the ARC CDC 7600; restrictions on storage space and computer costs require that we deal with a 64^3 approximation to these results, which is obtained by retaining only the lower half of the wavenumbers in each direction resolved in the 128^3 computation. Obviously, we lose details of the fine structure in this way, but the large scales which carry the bulk of the energy and which are responsible for most of turbulent transport are retained (90% of the energy in the 128^3 field is retained in our 64^3 representation).

We currently can produce contour plots in x-y, x-z, or y-z planes of each component of the turbulent stress (i.e., u^2, v^2, w^2, $-uv$, $-uw$, $-vw$), each component of the turbulent vorticity ω_i, and the square of the magnitude of the turbulent vorticity ω^2. In our investigation into the structure of this homogeneous shear flow, we have produced several planes of each of these quantities at several instants of time in its evolution.

We have only begun to make use of these "flow visualization" techniques, and any conclusions we could draw at this point are very preliminary. However, some interesting observations can be made, which are illustrated in figures 8-12. The results for the shear runs in these figures are for $St = 10$ (near the end of the portion of the simulation of this case which Rogallo claims to be adequately resolved) and are identified with the label SS1028

(St = 10, $\partial\bar{u}/\partial y = 28$). In these plots, contours of positive values of the quantity in question are shown with solid lines, negative values with dashed lines.

Figures 8(a) and (b) show contours in an x-y and x-z plane, respectively, of the predominant turbulent stress in this flow, -uv. The diagonal lines of figure 8(a) are drawn parallel to one of the principal axes for the turbulent stress in this flow field (calculated to lie at a 22° angle with respect to the x axis, ref. 1). These figures show some alignment of the contours with this principal axis, and none with the principal axis of the mean strain which is at 45°. Because the structures are, in the mean, inclined in x-y planes [fig. 8(a)], they appear somewhat shorter in the x-direction in x-z planes [fig. 8(b)]. Additionally, the structures appear somewhat thinner in the z-direction than in the direction normal to the principal axis in figure 8(a), suggesting that they resemble irregular "disks", with their thin dimension more or less aligned with the z axis. The relative "plumpness" of the structures in the x-y plane is counter to intuition; we had expected the structures to be sheared. By way of contrast, contours of -uv are shown in an x-y and x-z plane for an isotropic flow in figures 9(a) and (b). In this isotropic flow, no particular structure is apparent. (Note that the relative number of contours is not significant in the comparison of the plots for these two flows since it reflects the arbitrary choice of contour levels used.)

Contours of -vw in an x-y plane of the shear flow [fig. 10(a)] again show alignment of the structures with the principal axis for stress, with a "thinness" normal to this axis perhaps more in keeping with one's expectations. The x-z plane for this quantity [fig. 10(b)] shows no particular structure. It is interesting to note that the average value of -vw in this flow field is about 2% of the average value of -uv. Because the contours of figure 10 are at the same intervals as those of figure 8, one can infer that the average lack of -vw in the flow field is not due to absence

of -vw in the field, but rather to cancellation of positive -vw by an almost equal abount of negative -vw.

Further samples of the results generated to date are shown in figures 11 and 12, where x-y and x-z planes of the x component (ω_1, fig. 11) and the z component (ω_3, fig. 12) of turbulent vorticity are shown. Long thin structures aligned with the principal axis in the x-y plane are again prevalent, as is a lack of any organization in the x-z plane. Something lacking in these plots and in others we have generated but have not included here is any indication of vortex pairing.

At this point in our study, the mechanisms responsible for the production of turbulent energy and the growth of the turbulence length scales are not clear; the most that can be ventured is that these mechanisms seem to be different than those acting in the inhomogeneous version of this flow, the mixing layer. The elucidation of the essential similarities and differences in these flows is scheduled to be continued under ONR sponsorship in another program.

4. DEVELOPING A MODEL OF TURBULENCE NEAR A WALL FROM SOLUTIONS OF THE NAVIER-STOKES EQUATIONS

Most of the work on the development of a model for turbulence near a wall has been reported in an interim technical report (ref. 6). The work will be briefly summarized herein. The model for the first time makes direct use of what is known of the structure of the flow in the vicinity of the wall. The model, which can lead to improvements in both Reynolds averaged and subgrid-scale turbulence models, is based on the solution of the Navier-Stokes equations in the viscous sublayer.

The major goal of the work is to determine velocity boundary conditions to be applied at the edge of the viscous sublayer. In the work reported in reference 6, time and space phase relationships in the edge boundary conditions were explored. Only first harmonics were included in the work reported in reference 6.

Subsequently, preliminary work has been done to include higher harmonics of the velocity fluctuations at the edge of the sublayer. The first-harmonic work was surprisingly successful, and shows that there is considerable potential for coherent-structure modeling as a means of computing the dynamics of viscous-sublayer turbulence.

During the course of exploring various velocity boundary conditions, it was realized that two separate components would be required to simulate realistically the dynamics of viscous sublayer turbulence. One component represents the small-scale eddies (SSE) responsible for the principal production of turbulence and Reynolds stress. The second component represents organized large-scale eddies (LSE) which interact with the small-scale eddies. The crux of this coherent eddy model is the construction of appropriate time- and space-dependent boundary conditions for the three fluctuating velocity components u_{e+}, v_{e+}, w_{e+} at the outer edge of the viscous sublayer (at $y = y_e$). A simple construction has been used to date for purposes of illustrating the potential and the main characteristics of this type of turbulence modeling. With all quantities expressed in conventional dimensionless wall variables, the velocity boundary conditions developed are

$$\begin{array}{lll} & \underline{\text{Component 1 — SSE}} & \underline{\text{Component 2 — LSE}} \\ u_{e+} = & 2\alpha_1 \sin N_1 T \sin \zeta & + \sqrt{2(\alpha^2 - \alpha_1^2)}\sin(N_{u2}T + \phi_{u2}) \\ v_{e+} = & -2\beta \sin N_1 T \sin \zeta & \\ w_{e+} = & 2\beta \cos N_1 T \cos \zeta & + \sqrt{2(\gamma^2 - \beta^2)}\sin\left(\frac{N_{u2}}{2} T + \phi_{w2}\right) \end{array} \qquad (12)$$

where α, β, and γ are the rms intensities of fluctuation for u_{e+}, v_{e+}, w_{e+}, respectively, N_1 is the mean frequency of SSE burst events (ejection/sweep events), N_{u2} is the mean frequency of LSE, $\zeta \equiv 2\pi Z/\lambda$ is the dimensionless spanwise distance variable, T is the dimensionless time, λ is the mean spacing between high-speed and low-speed streaks, α_1/α is the uv correlation coefficient

(0.45) at y_e, and ϕ_{u2} and ϕ_{w2} are phase angles. The flow model is periodic both in time and span. The values of the various constants used in the comparisons presented in reference 6 are listed in table 4.

The computational mesh used for calculations contained 17 equally-spaced points in the spanwise direction and 24 points in the vertical direction clustered near the wall and near the edge by the functions

$$y_i^o = \frac{1}{2}\left\{1 + \frac{1}{a}\tanh\left[\xi_i \tanh^{-1}(a)\right]\right\} \tag{13}$$

and

$$y_i = \frac{y_i^o}{y_N^o} y_e$$

where

$$\xi_i = \frac{2(i - 1)}{N + 3} - 1$$

for

$$i = 1,2,3,\cdots,N$$

and

$$a = 0.98$$

This construction of velocity boundary conditions was guided by experimental observations of organized sublayer structure made during the past two decades. For example, the sin ζ factor for u_{e+} corresponds to the observation of high- and low-speed streaks spaced spanwise a mean distance of λ apart, while the factors sin ζ, -sin ζ, and cos ζ in the u_{e+}, v_{e+}, and w_{e+} equations, respectively, correspond to a simple modeling of the observations of contra-rotating vortical motion near a wall. The absence of a phase angle in time between U_{e+} and v_{e+} corresponds to the observation that the uv correlation in the log region, and hence at $y = y_e$, is maximum with zero time delay between their respective signals. The 180° phase difference between u_{e+} and v_{e+}

corresponds to observations from conditional samples in the sublayer that u and v are 180° out of phase during the Reynolds-stress intensive ejection-sweep event. The 90° phase difference in time between v_e and w_e corresponds to the observation that the derivative $(\partial \overline{v_e^2}/\partial y)_e$ at the outer edge of the viscous sublayer is zero. A comparison of a number of turbulence characteristics computed from this simple model with those measured in experiments showed surprisingly good agreement at the Reynolds number investigated ($Re_\delta \approx 29{,}000$).

It is of interest to note that the two-component type of velocity boundary condition at the outer edge of the viscous sublayer is precisely compatible with the concept of "active" and "inactive" components of turbulent motion in the log region as characterized by Townsend (ref. 18) and Bradshaw (ref. 19). Component 1 is active, involving small-scale eddies, producing the Reynolds stress, being rotational, and being dependent on wall variables. Component 2 is inactive, involving large-scale eddies, producing energy but no Reynolds stress, being irrotational, and being dependent on outer variables. There is much experimental information that turbulent flow comprises these two distinct types of motion in the log region, and hence at the outer edge of the viscous sublayer where the boundary conditions are applied.

Some preliminary runs were made for $Re_\delta = 11{,}000$, as well as for $Re_\delta = 29{,}000$. The results were not significantly different for this relatively small range of Re_δ, and only the computations for $Re_\delta = 29{,}000$ were presented in reference 6. These latter computations correspond essentially to the Re_δ of Laufer's classical pipe-flow experiments (ref. 20), and the Re_δ near which many other viscous-sublayer experiments were conducted. It is believed that computations over a wide range of Re_δ should be delayed until the intermittent production of Reynolds stress can be properly built into the velocity boundary conditions. Computations at high Re_δ will require much larger amounts of computer time. A run for $Re_\delta = 29{,}000$ takes about 4-5 minutes on the

CDC 7600 computer, while a run for Re_δ = 290,000 will take roughly 45 minutes. Hence it is prudent to essentially complete the model development before runs at very high Re_δ are made.

Computations at Re_δ = 29,000 were made for two different pressure gradients corresponding to pipe flow and channel flow. The results, presented in reference 6, showed that, for the mild pressure gradients of these two flows, the dynamics of viscous sublayer turbulence are nearly indistinguishable from those for zero pressure gradient on a flat plate. These results are consistent with experimental observations for which measuring inaccuracies have masked the very small differences in viscous sublayer flow which exist between pipes, channels, and flat plates.

In work done subsequent to the interim report (ref. 6), the computer program was modified to compute the spatial derivatives of velocity that determine the rate of energy dissipation. No results were obtained to evaluate the ability of the model to calculate the dissipation.

The primary weakness of the model reported in reference 6, as mentioned briefly earlier, is that it does not simulate the known physics of intermittent Reynolds stress production. The initial model corresponds to Reynolds stress being produced in a simple sinusoidal fashion with time; whereas in reality the viscous sublayer is quiescent most of the time and almost all of the Reynolds stress is produced in about 10-20 percent of the time through energetic burst/sweep events. Thus the main objective of work to improve the model is to develop modified velocity boundary conditions that simulate realistically the observed intermittent nature of Reynolds stress production.

The concept for accomplishing this objective is relatively simple. Reynolds stress is produced only by the active component of small-scale eddies (SSE); hence only the time function $\sin N_1 T$ in the boundary condition for u_{e+} and v_{e+} (and perhaps also the $\cos N_1 T$ function for w_{e+}) will need to be modified. The proposed

method of modification is illustrated in figure 13. Additional harmonics of the Fourier series that approximates a step-function burst/sweep event have been added to the sin N_1T term in the velocity boundary conditions in order to simulate intermittent production of Reynolds stress. Studies of the time and spatial phase relationships of the new boundary conditions are scheduled to be conducted under ONR sponsorship in another program.

5. CONCLUDING REMARKS

Studies have been conducted on several aspects of the structure and computation of incompressible turbulence. In the first of these, involving the testing in strained and sheared turbulence of subgrid-scale models for use in the large-eddy simulation of homogeneous turbulent flows, it has been shown that eddy viscosity models are quite inaccurate when severe strain has been imposed on the flow. If the model is to be used in strained or sheared turbulence despite this, it is better to remove the mean strain or shear from the velocity field before the model is computed. The deficiency in eddy viscosity models appears to come from the fact that the principal axes of the exact subgrid-scale stress and the modeled values are not aligned. New models based on the notion of scale similarity have been tested and, when used in combination with other models to provide energy dissipation, appear to offer considerable promise. And finally, it has been observed that when the strain is strong, the energy cascade is from the small scales to the larger ones, a result with possible considerable importance for turbulence modeling.

The second study involves the search for the mechanism underlying the growth of scales in homogeneous shear flow. Data management and computer-graphic routines have been developed to allow "flow-visualization-like" examination of flow fields calculated by full numerical simulation of the Navier-Stokes equations. Preliminary work accomplished to date in this study

suggests that the mechanisms controlling homogeneous shear flow are different than those underlying the inhomogeneous version of this flow, the mixing layer.

The third study, that of flow in the viscous sublayer revealed a good potential for constructing quantitative models of viscous sublayer turbulence founded on experimental observations of the physics of organized quasi-periodic eddy structures. Much physical information has been accumulated in the past two decades on organized sublayer structures. A sizeable part, but not all of the essential physics, has been included in the initial model. Embodiment of physics of coherent structures, however, has not been possible within the framework of conventional Reynolds-average modeling. It is clear that the present approach to modeling can be applied to study, for example, the effects of Reynolds number on turbulence intensities, dissipation, etc., as well as the effects of pressure gradients much stronger than those encountered in channel and pipe flow. Moreover, the method can be extended to more general conditions, such as to flows with heat transfer and compressibility. Modeling the effects of streamwise surface curvature, however, would apparently require extension to full three-dimensional flow by including the streamwise velocity derivatives neglected in the initial model.

REFERENCES

1. Rogallo, R. S.: Numerical Experiments in Homogeneous Turbulence. NASA TM 81315, Sept. 1981.

2. Ferziger, J. H. and McMillan, O. J.: Testing of Turbulence Models by Exact Numerical Solution of the Navier-Stokes Equations. NEAR TR 155, Nov. 1977.

3. McMillan, O. J. and Ferziger, J. H.: Direct Testing of Subgrid-Scale Models. NEAR TR 174, Nov. 1978.

4. McMillan, O. J. and Ferziger, J. H.: Direct Testing of Subgrid-Scale Models. AIAA Journal, Vol. 17, No. 12, Dec. 1979, pp. 1340-1346.

5. McMillan, O. J., Ferziger, J. H., and Rogallo, R. S.: Tests of Subgrid-Scale Models in Strained Turbulence. AIAA-80-1339, Jul. 1980.

6. Chapman, D. R. and Kuhn, G. D.: Two-Component Navier-Stokes Computational Model of Viscous Sublayer Turbulence. NEAR TR 278, Sept. 1982 (also AIAA Paper 81-1024, Jun. 1981).

7. Tucker, H. J. and Reynolds, A. J.: The Distortion of Turbulence by Irrotational Plane Strain. J. Fluid Mech., Vol. 32, Part 4, 1968, pp. 657-673.

8. Ferziger, J. H. and Shaanan, S.: Effect of Anisotropy and Rotation on Turbulence Production. Phys. Fluids, Vol. 19, Apr. 1976, pp. 596-597.

9. Leslie, D. C. and Quarini, G. L.: The Application of Turbulence Theory to the Formulation of Subgrid Modeling Procedures. J. Fluid Mech., Vol. 91, Part 1, 1979, pp. 65-91.

10. Shirani, E., Ferziger, J. H., and Reynolds, W. C.: Mixing of a Passive Scalar in Isotropic and Sheared Homogeneous Turbulence. Report No. TF-15, Dept. of Mech. Eng., Stanford University, Stanford, CA, May 1981.

11. Clark, R. A., Ferziger, J. H., and Reynolds, W. C.: Evaluation of Subgrid-Scale Turbulence Models Using a Fully Simulated Turbulent Flow. Report TF-9, Dept. of Mech. Eng., Stanford University, Stanford, CA, Mar. 1977.

12. Schumann, U.: Ein Verfahren zur direkten numerischen Simulation turbulenter Strömungen in Platten- und Rignspaltkanalen und über seine Anwendung zur Intersuchung von Turbulenzmodellen. Ph.D. Thesis, Karlsruhe University, 1973.

13. Deardorff, J. W.: A Numerical Study of Three-Dimensional Turbulent Channel Flow at Large Reynolds Numbers. J. Fluid Mech., Vol. 41, Part 2, pp. 452-480.

14. Moin, P., Reynolds, W. C., and Ferziger, J. H.: Large-Eddy Simulation of an Incompressible Turbulent Channel Flow. Rept. No. TF-12, Dept. of Mech. Eng., Stanford University, Stanford, CA, May 1978.

15. Kim, J. and Moin, P.: Large Eddy Simulation of Turbulent Channel Flow. Paper presented at AGARD Symposium, Turbulent Boundary Layers – Experiment, Theory, and Modeling. Sept. 24-27, 1979, The Hague, Netherlands.

16. Bardina, J., Ferziger, J. H., and Reynolds, W. C.: Improved Subgrid-Scale Models for Large-Eddy Simulation. AIAA Paper 80-1357, 1980.

17. Bardina, J.: Ph.D. Dissertation in preparation, Dept. of Mech. Eng., Stanford University, Stanford, CA.

18. Townsend, A. A.: Equilibrium Layers and Wall Turbulence. J. Fluid Mech., Vol. 11, Part 1, 1961, pp. 97-120.

19. Bradshaw, P.: Inactive Motion and Pressure Fluctuations in Turbulent Boundary Layers. J. Fluid Mech., Vol. 30, Part. 2, 1967, pp. 241-258.

20. Laufer, J.: The Structure of Turbulence in Fully Developed Pipe Flow. NACA TN 1174, 1954.

TABLE 1.- ENERGY TRANSFER TO THE SUBGRID-SCALES BY τ_{ij} AND $\tilde{\tau}_{ij}$. STRAIN RATIO = 4.

Grid	Γ (sec^{-1})	$\langle \tilde{\tau}_{ij} \frac{\partial \bar{u}_i}{\partial x_j} \rangle$ ($cm^2\ sec^{-3}$)	$\langle \tau_{ij} \frac{\partial \bar{u}_i}{\partial x_j} \rangle$ ($cm^2 sec^{-3}$)
64^3	5.30	-2.85	3.62
64^3	10.61	-4.77	-0.18
128^3	10.61	-8.30	-4.63

TABLE 2.- CORRELATION COEFFICIENTS, ISOTROPIC DECAY (R_{sgs} = 143).

	Smagorinsky	Equation (10)
Tensor	0.30	0.52
Vector	0.27	0.46
Scalar	0.37	0.45

TABLE 3.- CORRELATION COEFFICIENTS, PLANE STRAIN ($e^{\Gamma t}$ = 4.01, Γt_d = 3.75).

	Smagorinsky	Equation (10)
Tensor	0.11	0.49
Vector	0.11	0.47
Scalar	-0.09	0.45

TABLE 4.- VALUES OF CONSTANTS USED IN INITIAL MODEL OF TURBULENCE IN THE VISCOUS SUBLAYER.

$$\alpha = 2.0$$

$$\alpha_1 = 0.9$$

$$\beta = 1.0$$

$$\gamma = 1.3$$

$$N_1 = .025$$

$$N_{u2} = .025$$

$$\phi_{u2} = \pi/3$$

$$\phi_{w2} = 3\pi/4$$

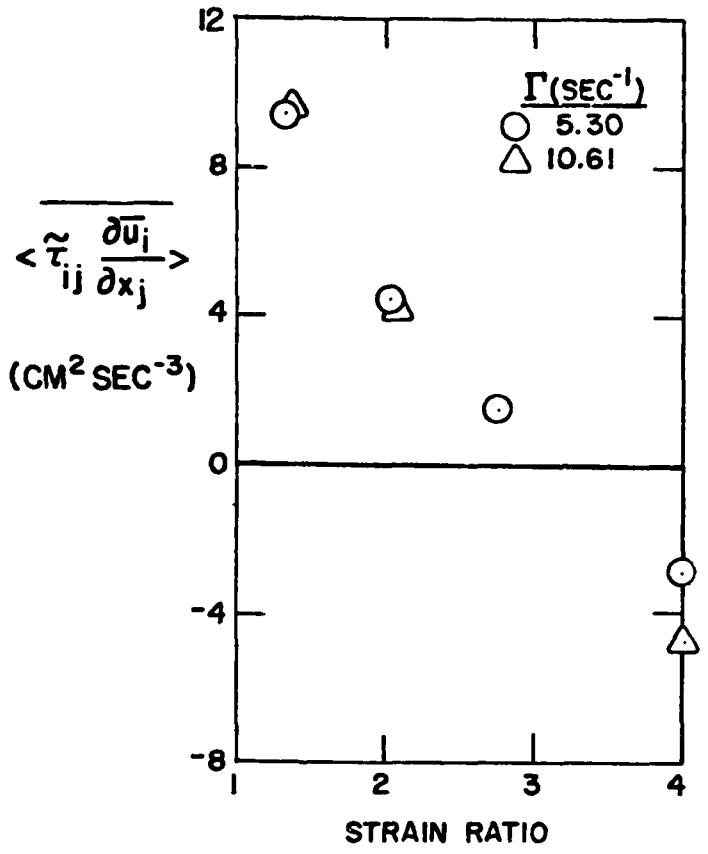

Figure 1.- Energy transfer via backscatter.

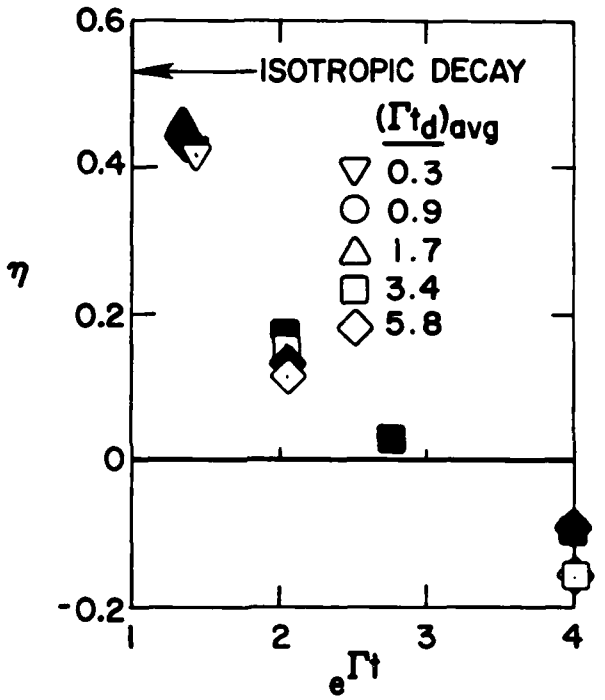

Figure 2.- Scalar correlations for Smagorinsky model.
Open symbols: mean strain rate included in model.
Closed symbols: no mean strain rate in model.

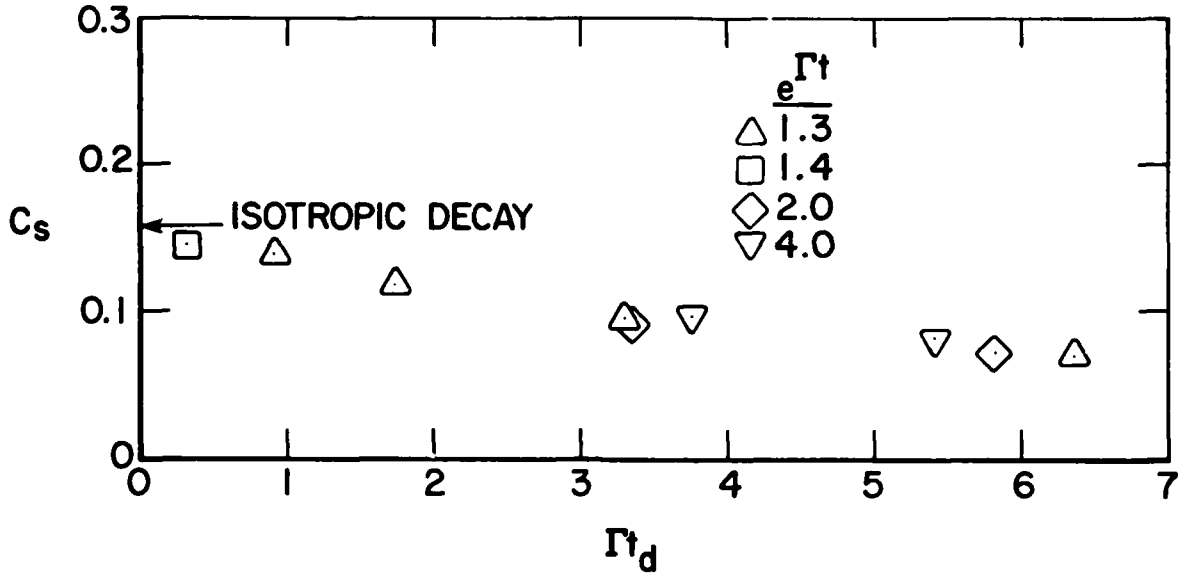

Figure 3.- Scalar-level parameter, Smagorinsky model. Mean strain rate included in model.

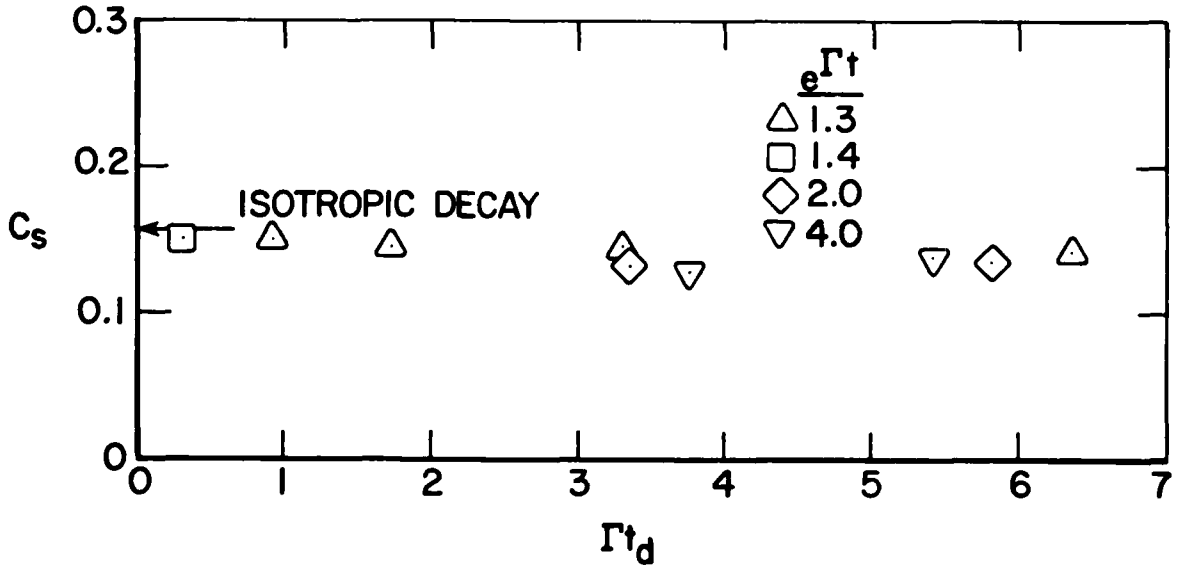

Figure 4.- Scalar-level parameter, Smgorinsky model. No mean strain rate in model.

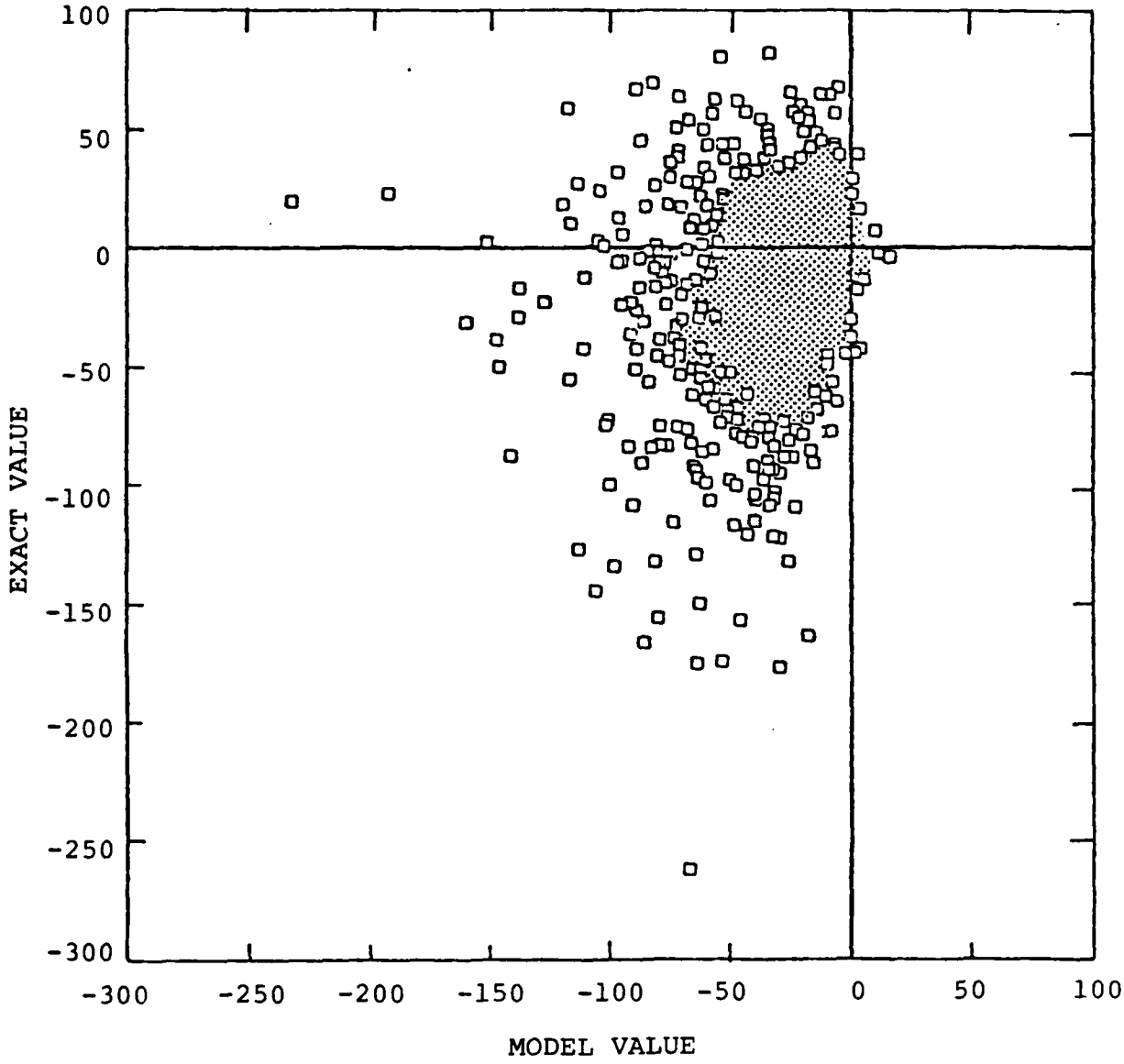

Figure 5.- Scatter plot of $\bar{u}_i \frac{\partial \tilde{\tau}_{ij}}{\partial x_j}$, Smagorinsky model, $e^{\Gamma t} = 1.32$, $\Gamma t_d = 0.92$.

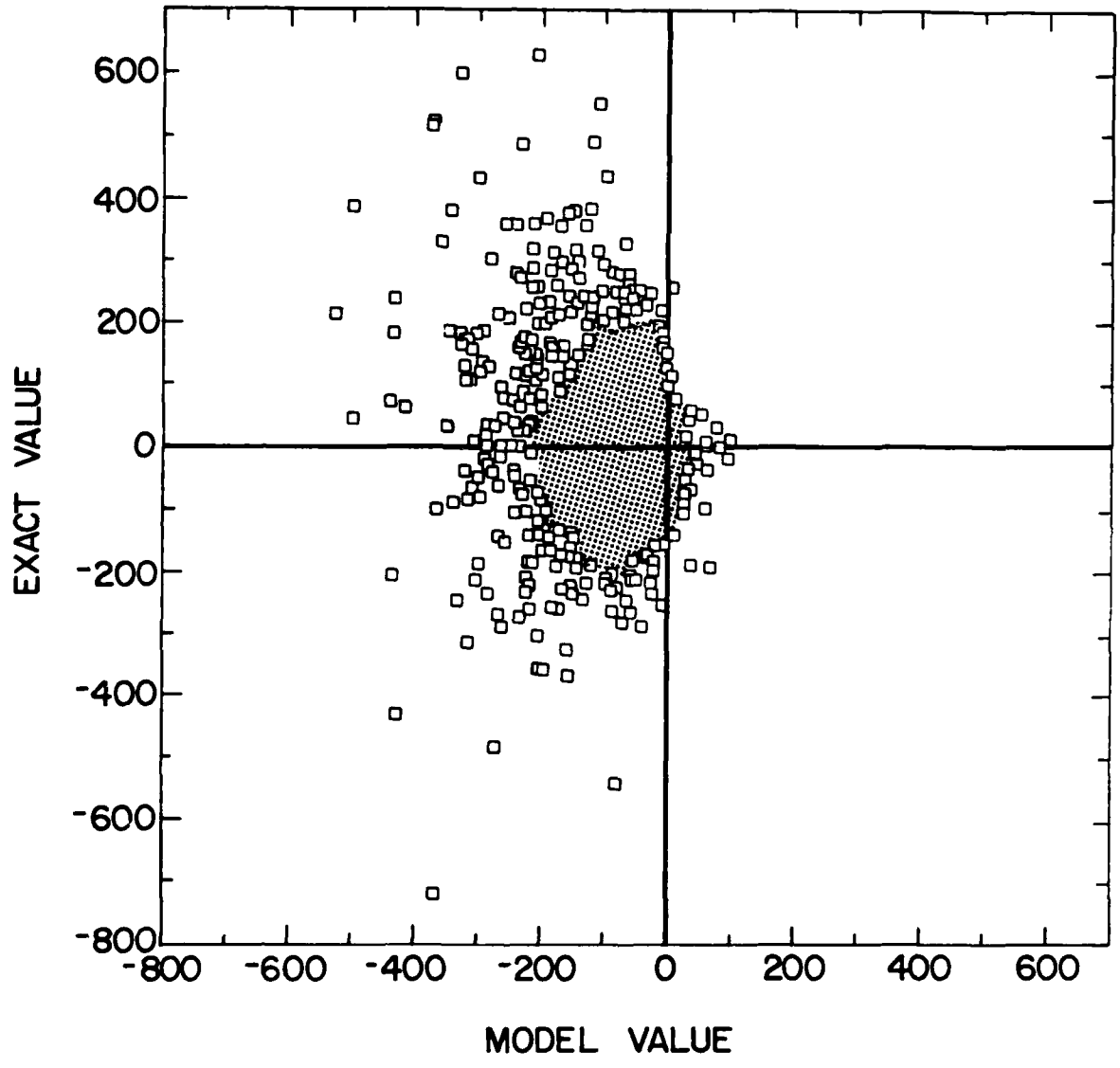

Figure 6.- Scatter plot of $\bar{u}_i \frac{\partial \tilde{\tau}_{ij}}{\partial x_j}$, Smagorinsky model, $e^{\Gamma t} = 4.01$, $\Gamma t_d = 3.75$.

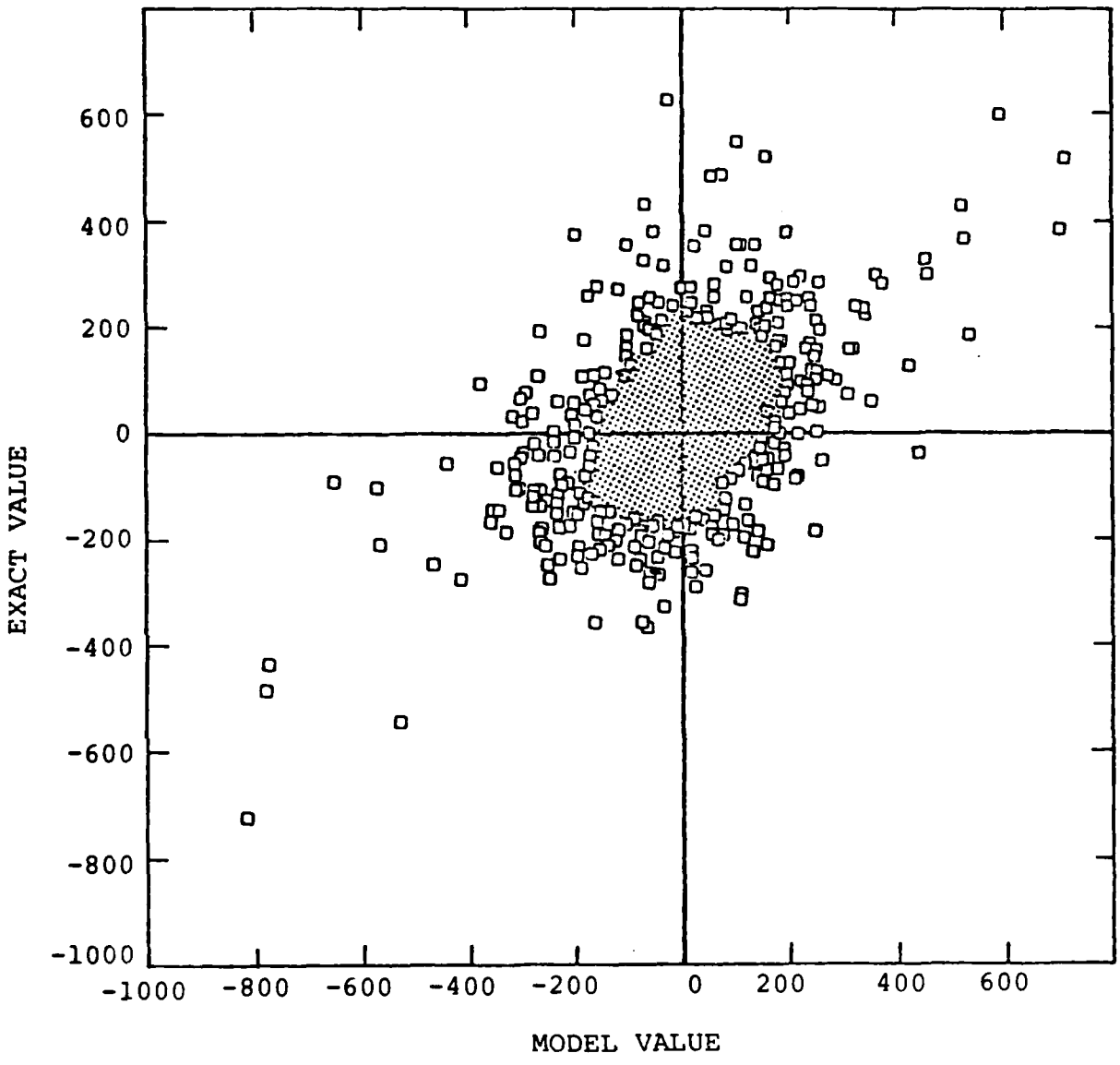

Figure 7.- Scatter plot of $\bar{u}_i \frac{\partial \tilde{\tau}_{ij}}{\partial x_j}$, model of eq. (10), $e^{\Gamma t} = 4.01$, $\Gamma t_d = 3.75$.

CONTOURS OF -UV

SS1028 SHEAR RUN

X-Y PLANE NUMBER 32

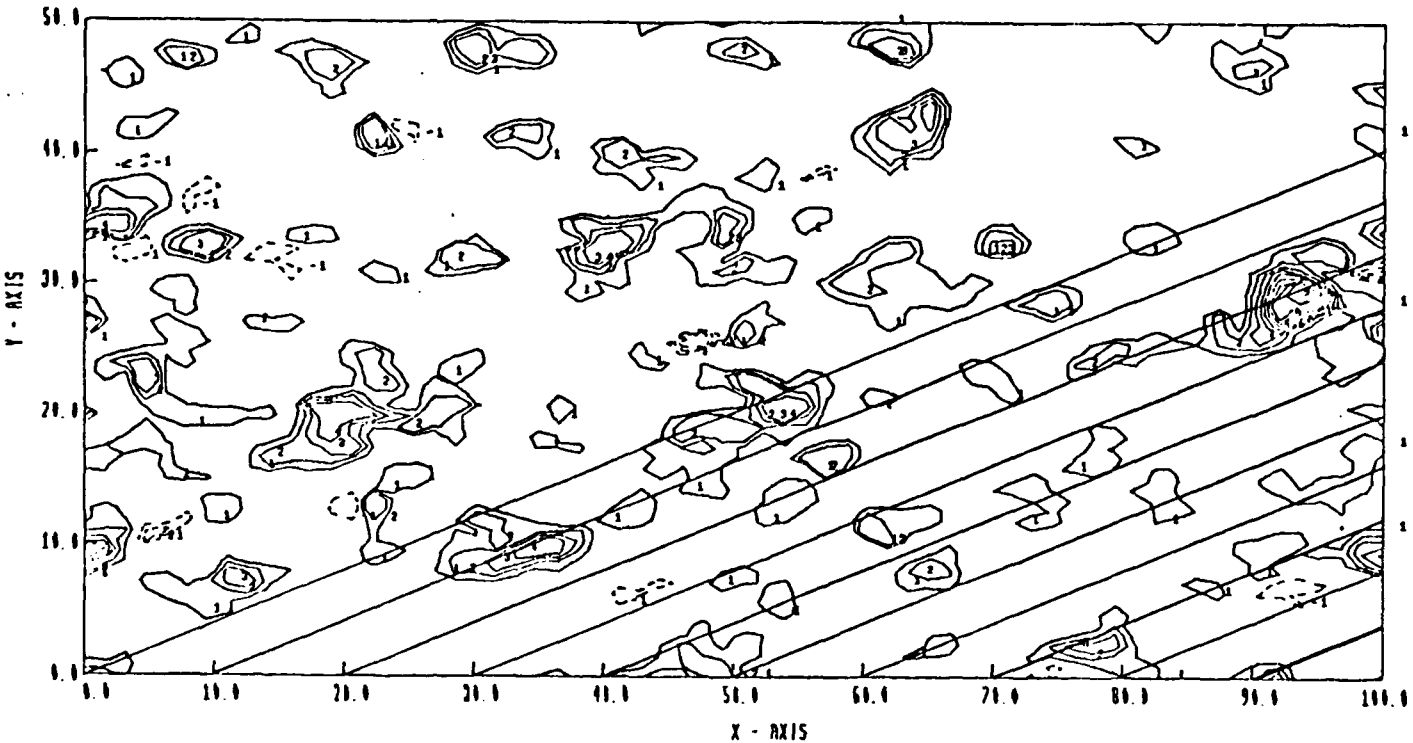

Figure 8(a)

CONTOURS OF -UV

SS1028 SHEAR RUN

X-Z PLANE NUMBER 32

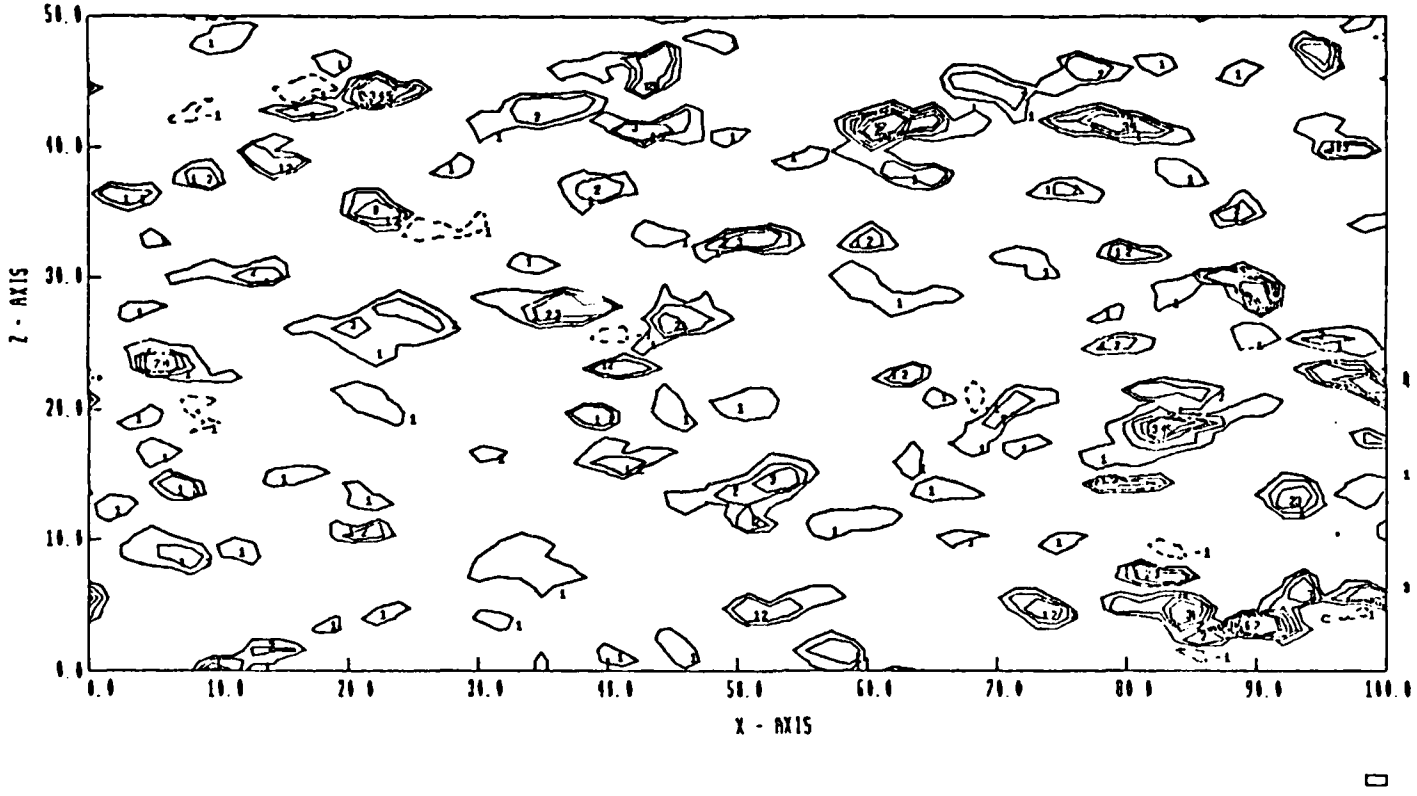

Figure 8(b)

RE3840N ISOTROPIC RUN

X-Y PLANE NUMBER 32

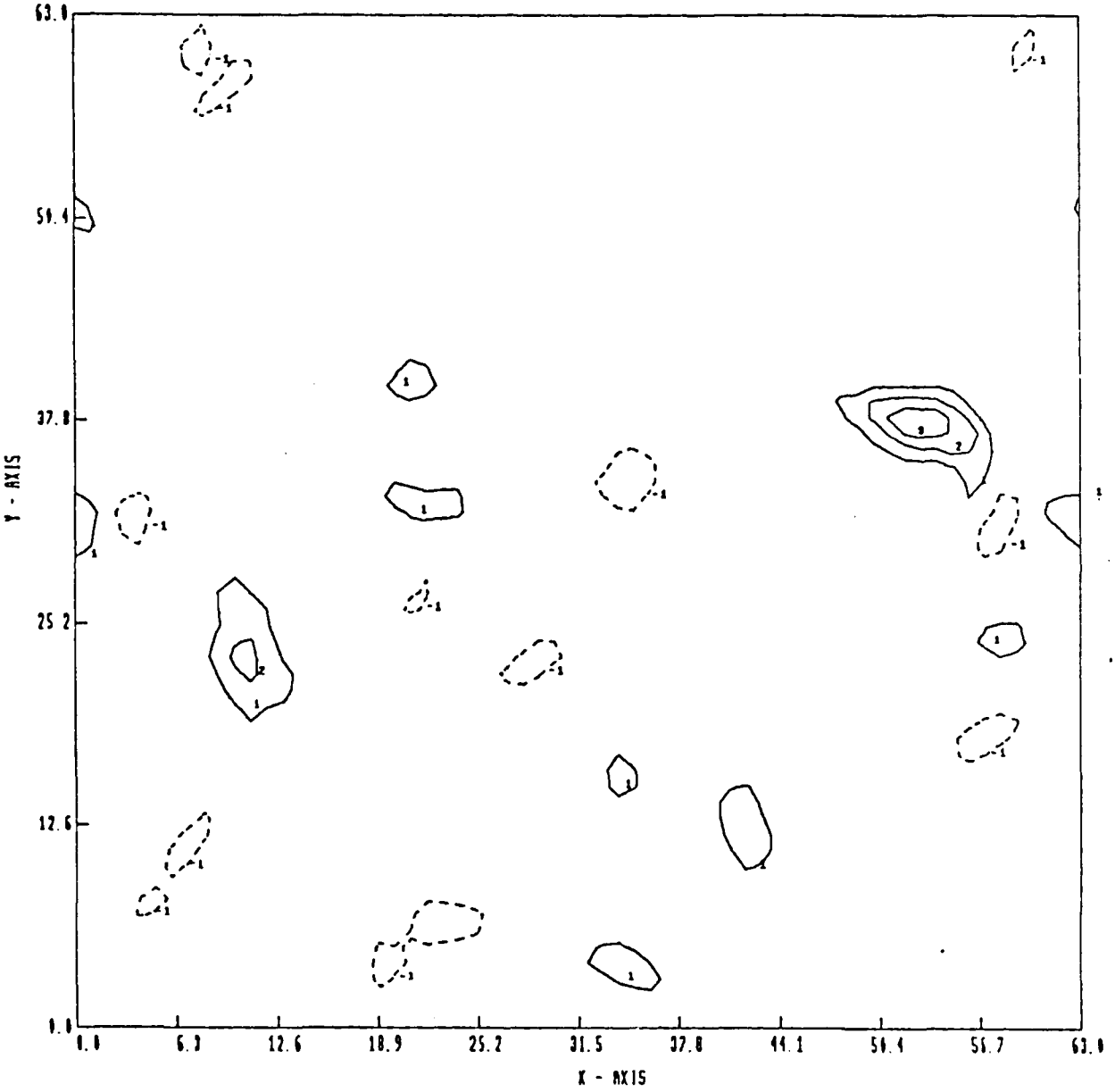

Figure 9(a)

CONTOURS OF -UV

RE3840N ISOTROPIC RUN

X-Z PLANE NUMBER 32

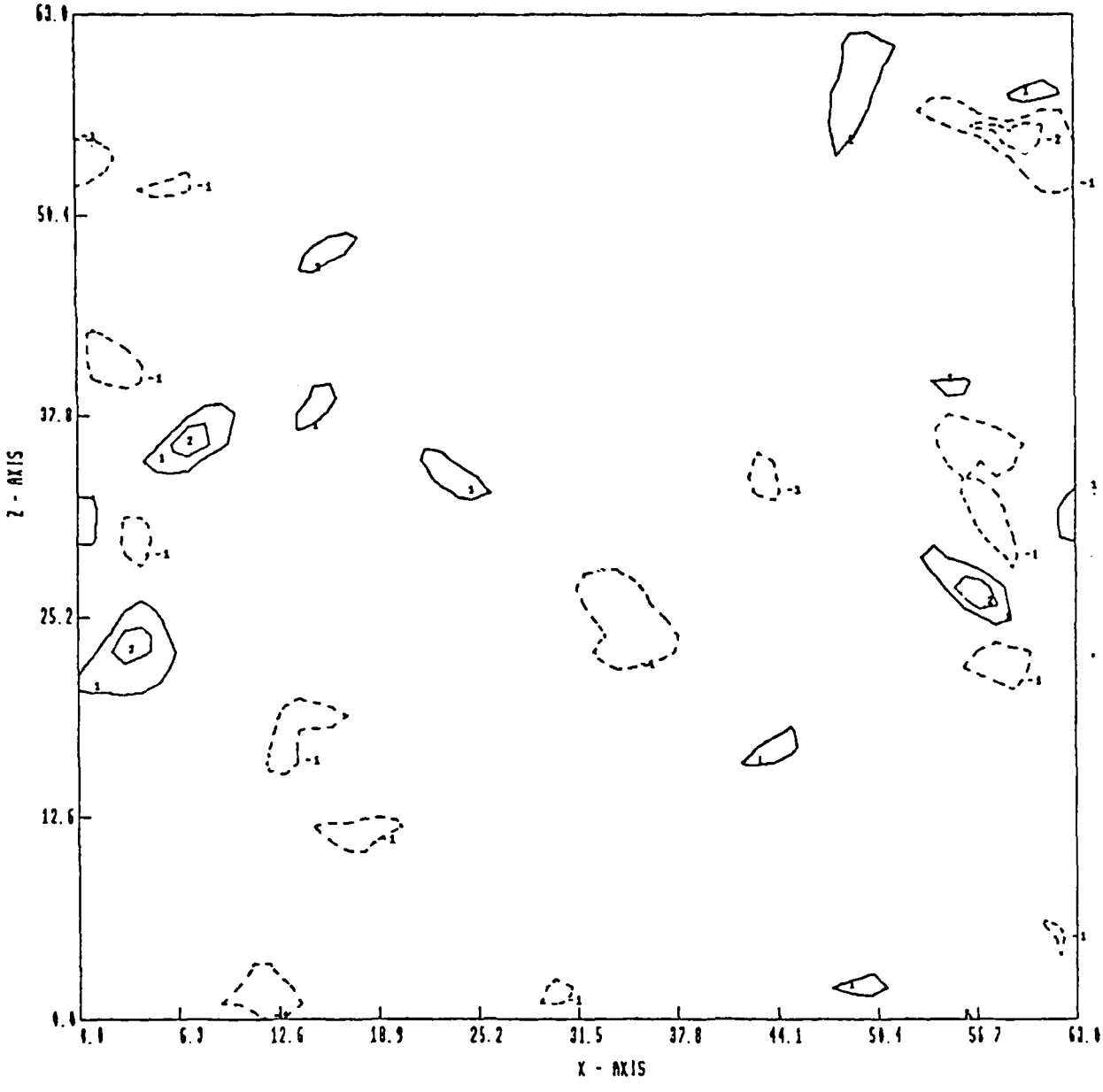

Figure 9(b)

CONTOURS OF -UV

CONTOURS OF -VW

SS1028 SHEAR RUN

X-Y PLANE NUMBER 32

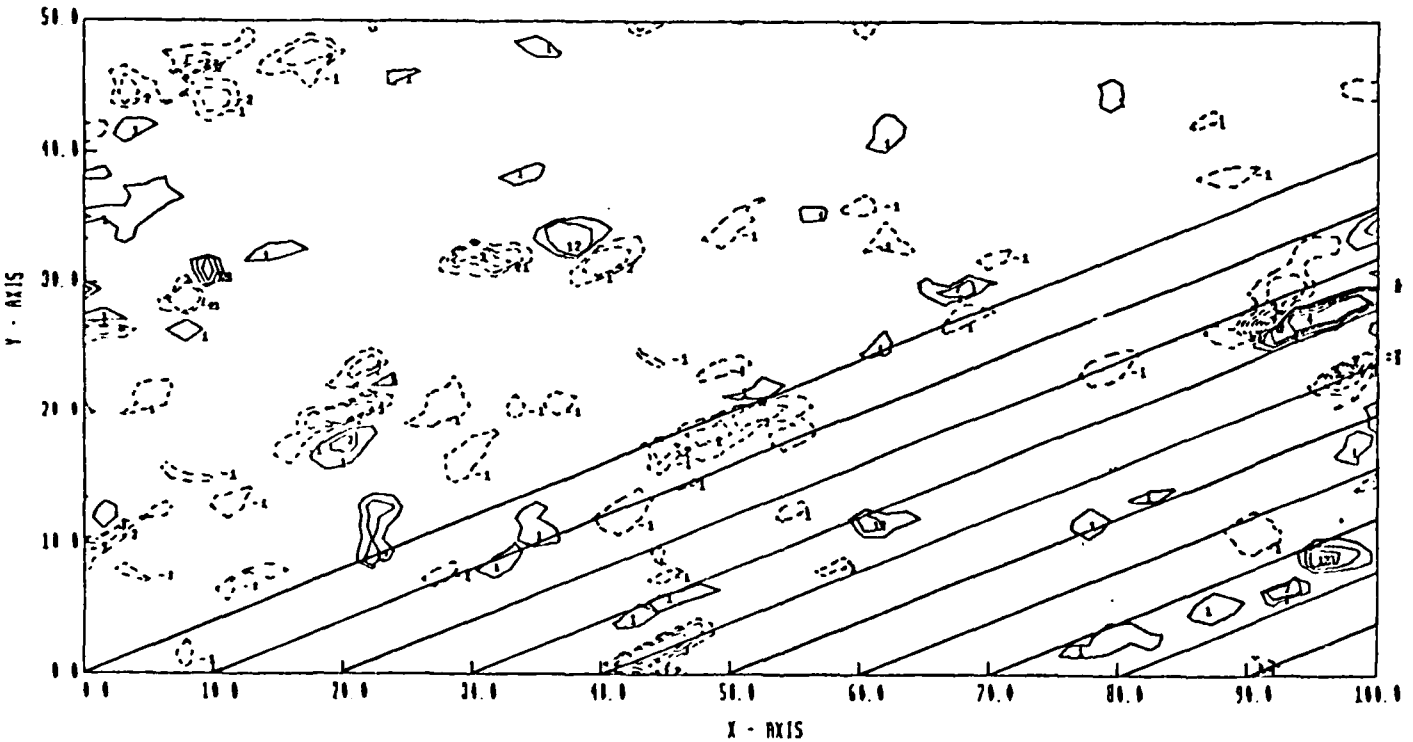

Figure 10(a)

CONTOURS OF -VW

SS1028 SHEAR RUN

X-Z PLANE NUMBER 32

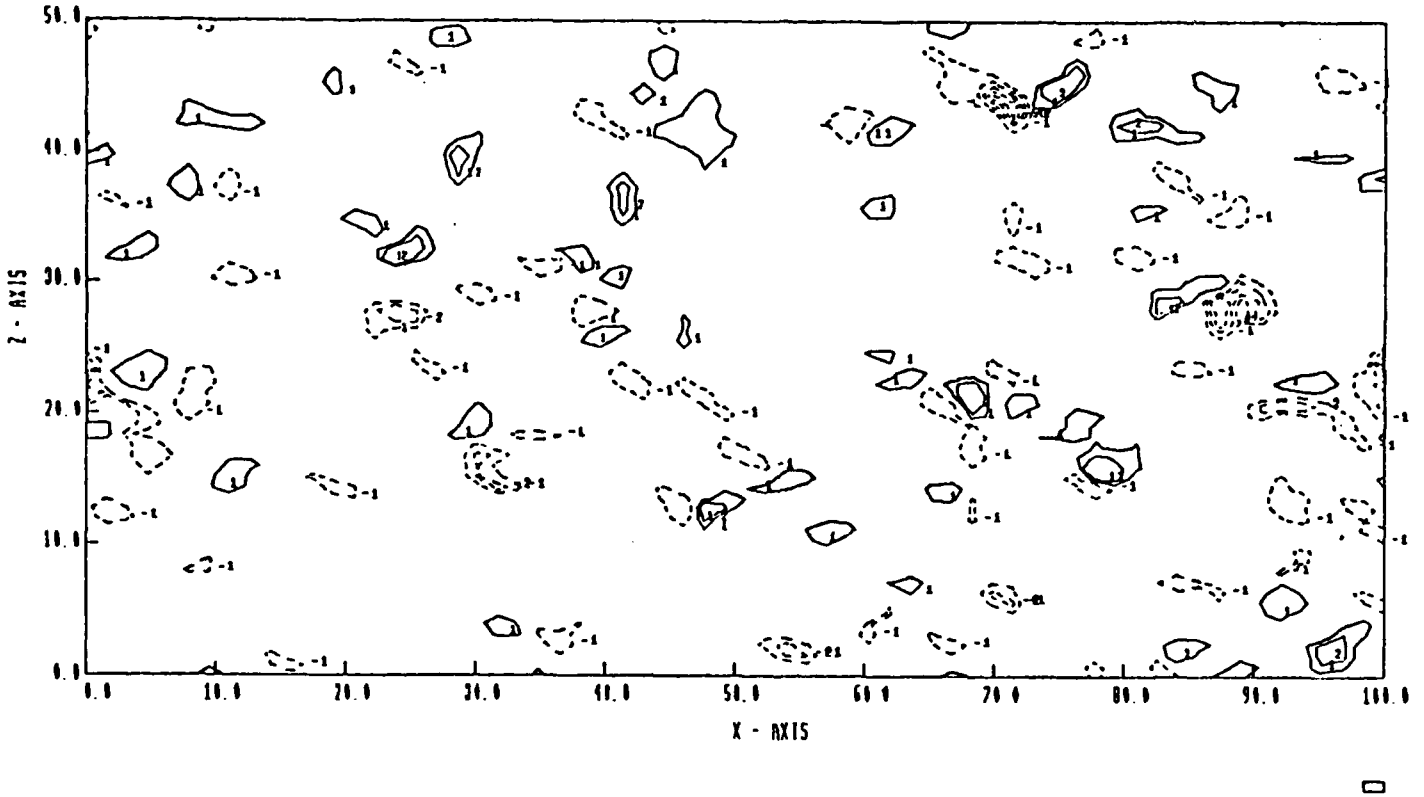

Figure 10(b)

CONTOURS OF X VORTICITY

SS1028 SHEAR RUN

X-Y PLANE NUMBER 32

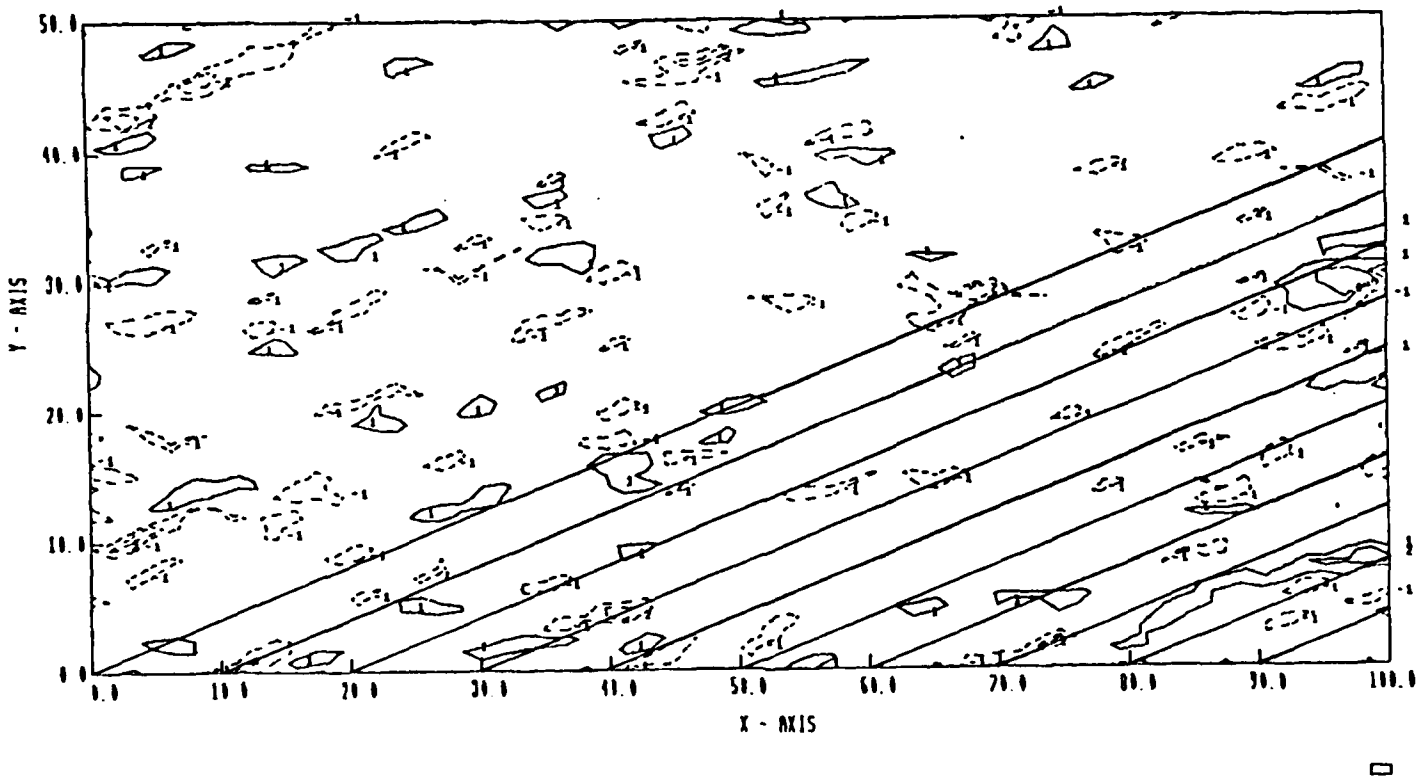

Figure 11(a)

CONTOURS OF X VORTICITY

SS1028 SHEAR RUN

X-Z PLANE NUMBER 32

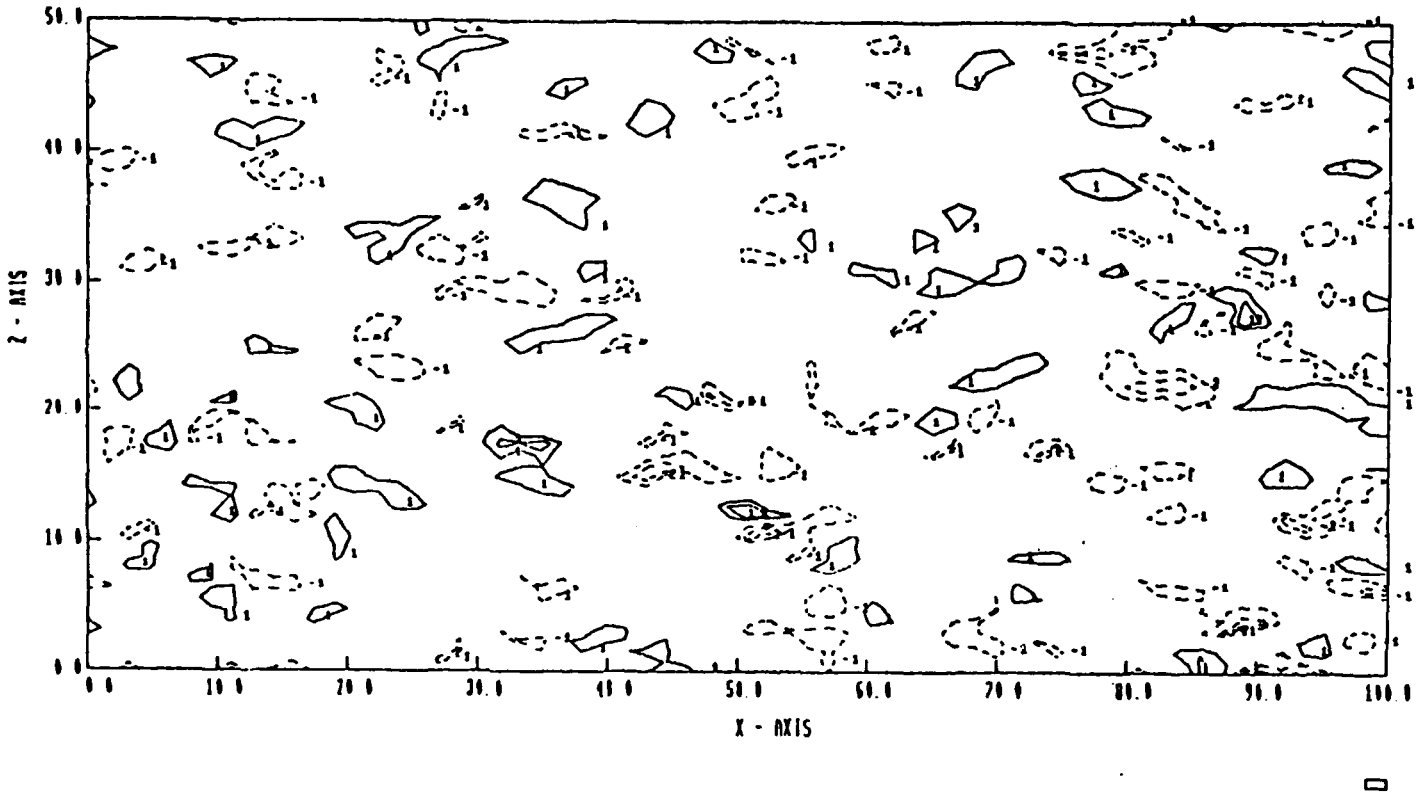

Figure 11(b)

CONTOURS OF Z VORTICITY

SS1028 SHEAR RUN

X-Y PLANE NUMBER 32

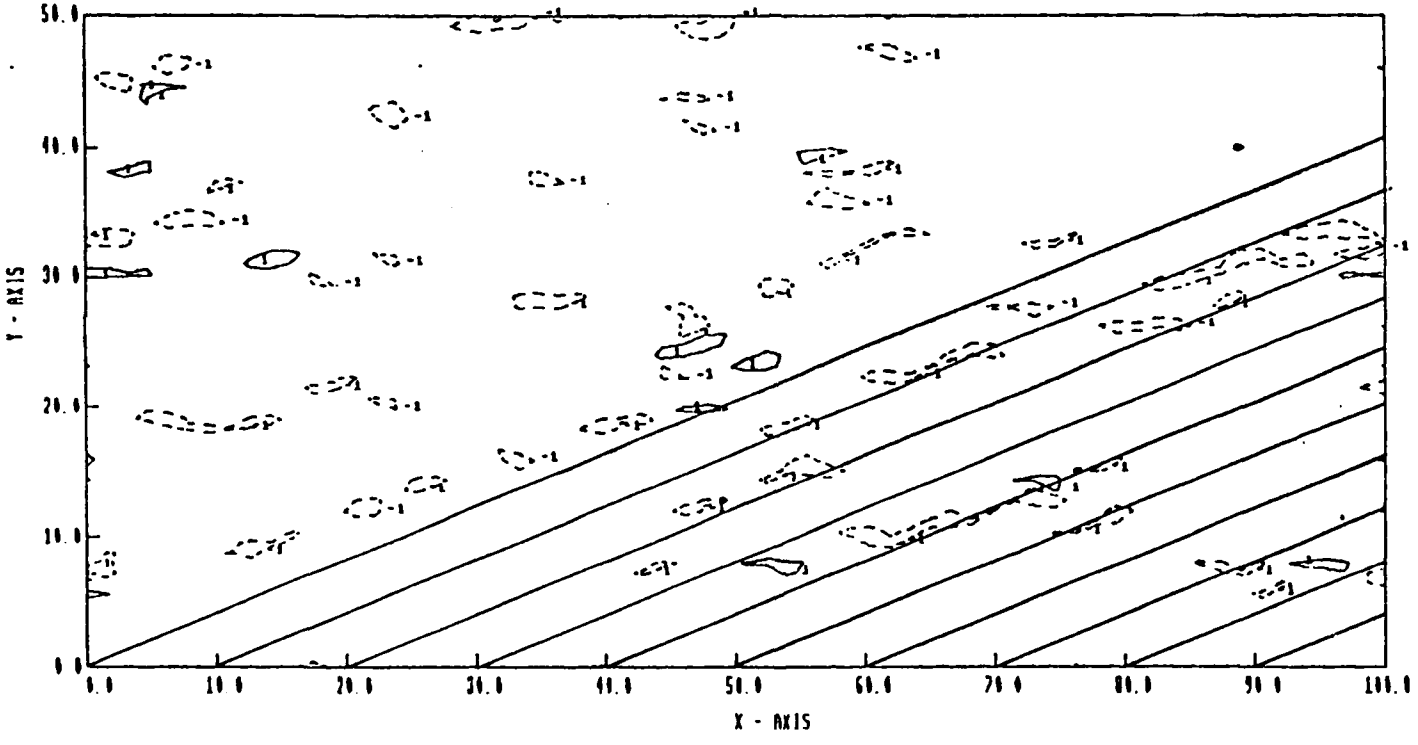

Figure 12(a)

CONTOURS OF Z VORTICITY

SS1028 SHEAR RUN

X-Z PLANE NUMBER 32

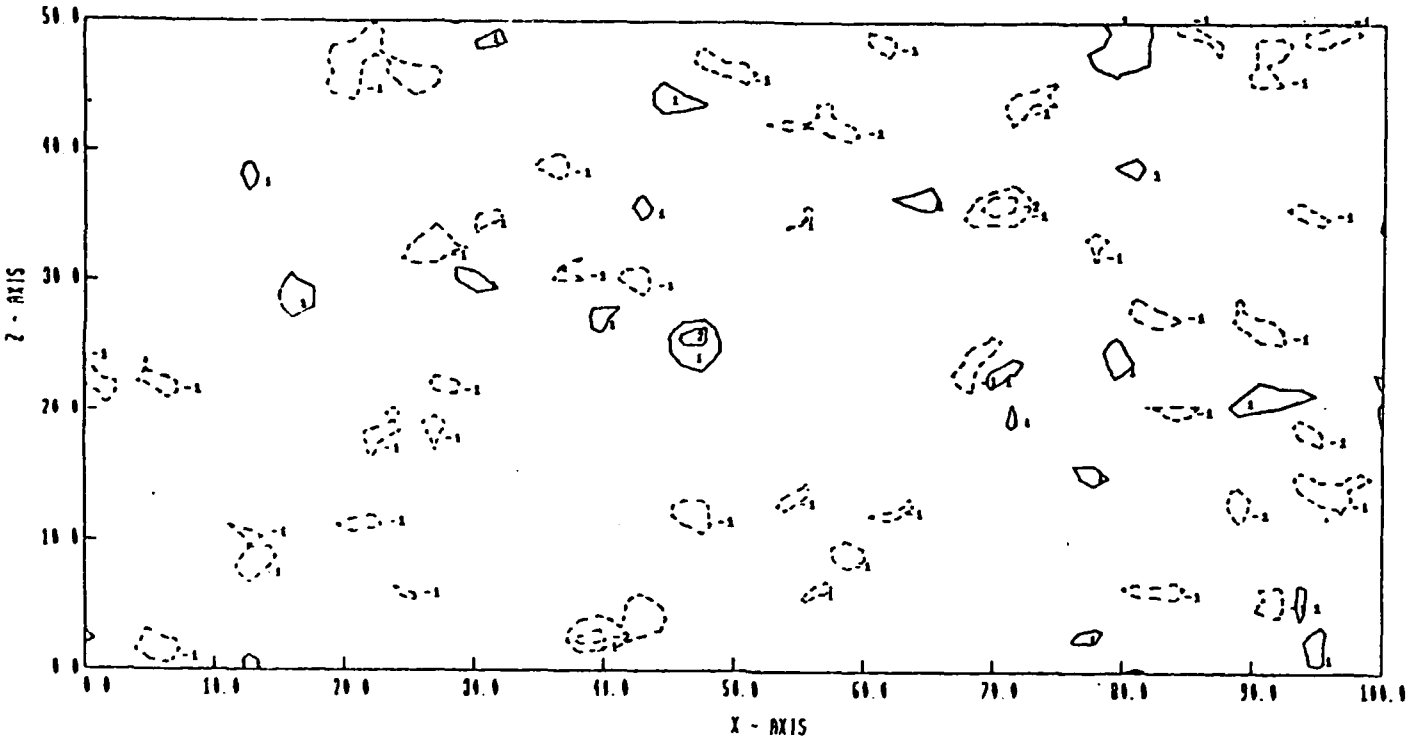

Figure 12(b)

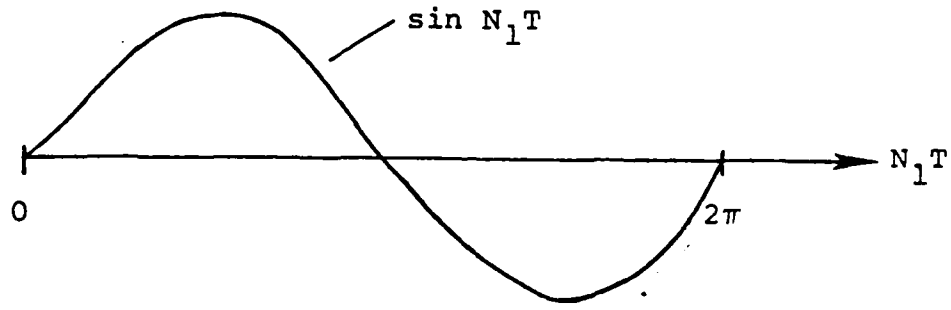

(a) present model

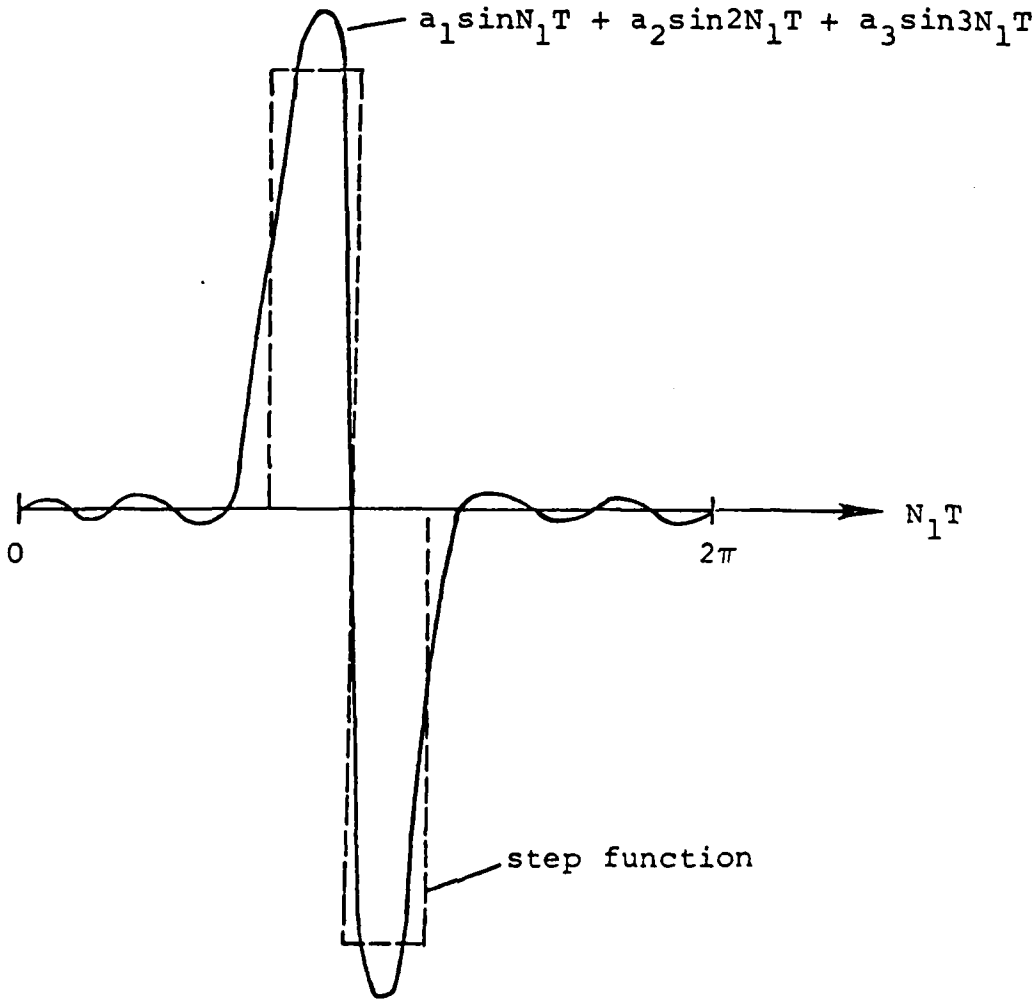

(b) Proposed model for simulating intermittent Reynolds stress production.

Figure 13.- Time variation functions for component-1 small-scale eddies in the boundary conditions for u_{e+} and v_{e+}.

DISTRIBUTION LIST

Technical Library
Building 313
Ballistic Research Laboratories
Aberdeen Proving Ground, MD 21005

Defense Technical Information Center 12
Cameron Station, Building 5
Alexandria, VA 22314

Library
Naval Academy
Annapolis, MD 21402

Director, Tactical Technology Office
Defense Advanced Research Projects Agency
1400 Wilson Boulevard
Arlington, VA 22209

Code 200B
Office of Naval Research
800 N. Quincy Street
Arlington, VA 22217

Code 438 2
Office of Naval Research
800 N. Quincy Street
Arlington, VA 22217

Dr. J. L. Potter
Deputy Director, Technology
von Karman Gas Dynamics Facility
Arnold Air Force Station, TN 37389

Professor J. C. Wu
School of Aerospace Engineering
Georgia Institute of Technology
Atlanta, GA 30332

NASA Scientific and Technical Information Facility
P.O. Box 8757
Baltimore/Washington International Airport, MD 21240

Dr. T. C. Tai
Code 1606
David W. Taylor Naval Ship Research and Development Center
Bethesda, MD 20084

Dr. G. R. Inger
Department of Aerospace Engineering
University of Colorado
Boulder, CO 80309

Professor A. H. Nayfeh
Department of Engineering Science
Virginia Polytechnic Institute and State University
Blacksburg, VA 24061

Dr. A. Rubel
Research Department
Grumman Aerospace Corporation
Bethpage, NY 11714

Commanding Officer
Office of Naval Research Eastern/Central Regional Office
666 Summer Street, Bldg. 114, Section D
Boston, MA 02210

Commanding Officer
Office of Naval Research Branch Office
536 South Clark Street
Chicago, IL 60605

Code 753
Naval Weapons Center
China Lake, CA 93555

Code 4063
Naval Weapons Center
China Lake, CA 93555

Professor R. T. Davis
Department of Aerospace Engineering
University of Cincinnati
Cincinnati, OH 45221

Library MS 60-3
NASA Lewis Research Center
21000 Brookpark Road
Cleveland, OH 44135

Dr. J. D. Anderson, Jr.
Chairman, Department of Aerospace Engineering
College of Engineering
University of Maryland
College Park, MD 20742

Professor O. Burggraf
Department of Aeronautical and
Astronautical Engineering
Ohio State University
1314 Kinnear Road
Columbus, OH 43212

Technical Library
Naval Surface Weapons Center
Dahlgren Laboratory
Dahlgren, VA 22448

Technical Library 2-51131
LTV Aerospace Corporation
P. O. Box 5907
Dallas, TX 75222

Library, United Aircraft Corporation
Research Laboratories
Silver Lane
East Hartford, CT 06108

Dr. W. R. Briley
Scientific Research Associates, Inc.
P. O. Box 498
Glastonbury, CT 06033

Library (MS 185)
NASA Langley Research Center
Langley Station
Hampton, VA 23665

Technical Library
Naval Ordnance Station
Indian Head, MD 20640

Professor E. L. Resler
Sibley School of Mechnical and
Aerospace Engineering
Cornell University
Ithaca, NY 14850

Library
Midwest Research Institute
425 Volker Boulevard
Kansas City, MO 64110

Dr. J. J. Riley
Flow Research, Inc.
P. O. Box 5040
Kent, WA 98031

Dr. P. Bradshaw
Imperial College of Science and
Technology
Department of Aeronautics
Prince Consort Road
London SW7 2BY, England

Professor T. Cebeci
Mechanical Engineering Department
California State University, Long
Beach
Long Beach, CA 90840

Engineering Library
University of Southern California
Box 77929
Los Angeles, CA 90007

Commanding Officer
Naval Ordnance Station
Louisville, KY 40214

Professor E. R. G. Eckert
University of Minnesota
241 Mechanical Engineering Building
Minneapolis, MN 55455

Dr. Gary Chapman
Mail Stop 227-4
Ames Research Center
Moffett Field, CA 94035

Library
Naval Postgraduate School
Monterey, CA 93940

Engineering Societies Library
345 East 47th Street
New York, NY 10017

Professor G. Miller
Department of Applied Science
New York University
26-36 Stuyvesant Street
New York, NY 10003

Office of Naval Research
New York Area Office
715 Broadway - 5th Floor
New York, NY 10003

Librarian, Aeronautical Library
National Research Council
Montreal Road
Ottawa 7, Canada

Lockheed Missiles and Space Company
Technical Information Center
3251 Hanover Street
Palo Alto, CA 94304

Commanding Officer
Office of Naval Research
Western Regional Office
1030 East Green Street
Pasadena, CA 91106

Engineering Division
California Institute of Technology
Pasadena, CA 91109

Library
Jet Propulsion Laboratory
4800 Oak Grove Drive
Pasadena, CA 91103

Professor H. Liepmann
Department of Aeronautics
California Institute of Technology
Pasadena, CA 91109

Mr. L. I. Chasen, MGR-MSD Lib.
General Electric Company
Missile and Space Division
P. O. Box 8555
Philadelphia, PA 19101

Technical Library
Naval Missile Center
Point Mugu, CA 93042

Professor S. Bogdonoff
Gas Dynamics Laboratory
Department of Aerospace and
Mechanical Sciences
Princeton University
Princeton, NJ 08540

Dr. J. E. Yates
Aeronautical Research Associates
of Princeton, Inc.
50 Washington Road
Princeton, NJ 08540

Redstone Scientific Information Center
Chief, Document Section
Army Missile Command
Redstone Arsenal, AL 35809

U.S. Army Research Office
P. O. Box 12211
Research Triangle, NC 27709

Editor, Applied Mechanics Review
Southwest Research Institute
8500 Culebra Road
San Antonio, TX 78228

Library and Information Services
General Dynamics - CONVAIR
P. O. Box 1128
San Diego, CA 92112

Office of Naval Research
San Francisco Area Office
One Hallidie Plaza, Suite 601
San Francisco, CA 94102

Library
The RAND Corporation
1700 Main Street
Santa Monica, CA 90401

Dr. P. E. Rubbert
Boeing Aerospace Company
Boeing Military Airplane Development
Organization
P. O. Box 3707
Seattle, WA 98124

Librarian
Naval Surface Weapons Center
White Oak Laboratory
Silver Spring, MD 20910

Engineering Library
McDonnell Douglas Corporation
Department 218, Building 101
P. O. Box 516
St. Louis, MO 63166

Dr. N. Malmuth
Rockwell International Science Center
1049 Camino Dos Rios
P. O. Box 1085
Thousand Oaks, CA 91360

Library
Institute of Aerospace Studies
University of Toronto
Toronto 5, Canada

Professor W. R. Sears
Aerospace and Mechanical Engineering
University of Arizona
Tucson, AZ 85721

Air Force Office of Scientific
Research (SREM)
Building 1410, Bolling AFB
Washington, DC 20332

Chief of Research and Development
Office of Chief of Staff
Department of the Army
Washington, DC 20310

Library of Congress
Science and Technology Division
Washington, DC 20540

Director of Research (Code RR)
National Aeronautics and Space
Administration
600 Independence Avenue, SW
Washington, DC 20546

Library
National Bureau of Standards
Washington, DC 20234

National Science Foundation
Engineering Division
1800 G. Street, NW
Washington, DC 20550

AIR 320D
Naval Air Systems Command
Washington, DC 20361

AIR 950D
Naval Air Systems Command
Washington, DC 20375

Code 2627 6
Naval Research Laboratory
Washington, DC 20375

SEA 03512
Naval Sea Systems Command
Washington, DC 20362

SEA 09G3
Naval Sea Systems Command
Washington, DC 20362

Dr. Charles Watkins
Head, Mechanical Engineering Dept.
Howard University
Washington, DC 20059

Dr. A. L. Slafkosky
Scientific Advisor
Commandant of the Marine Corps
(Code AX)
Washington, DC 20380

Director
Weapons Systems Evaluation Group
Washington, DC 20350

Research Library
AVCO Corporation
Missile Systems Division
201 Lowell Street
Wilmington, MA 01887

AFAPL (APRC)
AB
Wright Patterson AFB, OH 45433

Office of Naval Research 6
Department of the Navy
Attn: Code 102IP
Arlington, VA 22217